



Project 034 Overall Integration and Coordination

University of Dayton

Project Lead Investigator

Joshua Heyne
Assistant Professor
Mechanical Engineering
University of Dayton
300 College Park
Dayton, OH 45458
937 229-5319
Jheyne1@udayton.edu

University Participants

University of Dayton

- P.I.(s): Joshua Heyne, Scott Stouffer, and Alejandro Briones
- FAA Award Number: 13-C-AJFE-UD (Amendment Nos. 9, 10, 13, & 17)
- Period of Performance: September, 18 2015 to December, 31 2017
- Task(s):
 1. Overall NJFCP integration and coordination
 2. Well-Stirred Reactor experiments on LBO and Speciation
 3. Cross-experiment analysis
 4. Common format routine software and model development
 5. Spray modeling of Area 3 (GT P&W pressure atomizer)
 6. Cold ignition experiments in the Referee Rig of alternative fuel blends

Project Funding Level

Amendment No. 9: \$134,999.00 (September, 18 2015 to February, 28 2017)

Amendment No. 10: \$249,330.00 (July, 7 2016 to December, 31 2017)

Amendment No. 13: \$386,035.00 (August, 30 2016 to December, 31 2017)

Amendment No. 17: \$192,997.00 (August, 3 2017 to September, 30 2018)

Cost share is provided by GE Aviation (\$135,000.00), DLR Germany (\$512,924.00), United Technologies Research Center (\$150,000.00), ANSYS/FLUENT (\$175,000.00), and the University of Dayton (\$53,887.00) in to form of in-kind research at GE Aviation, DLR Germany, and United Technologies, direct financial support at the University of Dayton, and reduced software license fees at ANSYS/FLUENT.

Investigation Team

- Joshua Heyne (University of Dayton) is the Project Lead Investigator for coordinating all NJFCP teams (both ASCENT and non-ASCENT efforts), Well-Stirred Reactor experiments, procuring additional geometrical configurations, and leading studies across experimental platforms within the NJFCP.
- Scott Stouffer (University of Dayton Research Institute) is conducting ignition testing of NJFCP fuels in the Referee Rig.
- Alejandro Briones (University of Dayton Research Institute) is the P.I. responsible for leading the common format routine software development.
- Vaidya Sankaran (UTRC) is sub-contracted to conduct the spray modeling of the Area 3 pressure atomizing spray injector.



- Bob Olding (University of Dayton Research Institute) is part of the team managed by Alejandro Briones to develop the common format routine software. Mr. Olding's main task is on Scheme GUI/TUI programming for later use by OEM CFD teams.
- Mike Hanchak (University of Dayton Research Institute) is part of the team managed by Alejandro Briones to develop the common format routine software. Mr. Hanchak's main task is on CFD and combustion programming for later use by OEM CFD teams.
- Tyler Hendershott (University of Dayton Research Institute) is part of the team working on the ignition of conventional and alternative jet fuels in the Referee Rig.
- Jeffery Monfort (University of Dayton Research Institute) is part of the team working on the ignition of conventional and alternative jet fuels in the Referee Rig.
- Robert Stachler (University of Dayton) is a Ph.D. student conducting the Lean Blowout and emissions measurements in the Well-Stirred Reactor.
- Erin Peiffer (University of Dayton) is a Master's student linking experimental results across ASCENT and non-ASCENT teams.
- Jeremy Carson (University of Dayton) was a Master's student linking experimental results across ASCENT and non-ASCENT teams. Jeremy has since graduated and is now employed full time at UDRI.
- Sherri Alexander (University of Dayton) is an administrative assistant aiding in the compilation of meeting minutes and setting up teleconference times.
- Katherine Opacich (University of Dayton) is an undergraduate research assistant working to document NJFCP activities.

Project Overview

In total, the NJFCP is composed of more than two dozen member institutions contributing information and data as diverse as expert advice from gas turbine Original Equipment Manufacturers (OEMs), federal agencies, other ASCENT universities and corroborating experiments at DLR Germany, NRC Canada and other international partners etc. The project is tasked to coordinate and integrate amongst these diverse program stakeholders, academic Principle Investigators (PIs) and etc., cross-analyze results from other NJFCP areas, collect data for modeling and fuel comparison purposes in a Well-Stirred Reactor (WSR), conduct Large Eddy Simulations (LES) of sprays for the Area 3 High Sheer Rig, and procure additional swirler geometries for the NJFCP Areas and Allied Partners while developing interface of NJFCP modeling capabilities with OEM requirements. Work under this program consists of, but is not limited to:

- meetings with member institutions to facilitate the consistency of testing and modeling,
- coordinate timely completion of program milestones,
- documentation of results and procedures,
- creation of documents critical for program process (e.g. fuel down selection criteria)
- solicit and incorporate program feedback from OEMs,
- reporting and presenting on behalf of the NJFCP at meetings and technical conferences,
- integrate the state-of-the-art combustion and spray models into user-defined-functions (UDFs),
- WSR testing of NJFCP Category A, Category C, and Surrogate fuels,
- LES of sprays for A2, C1, and C5 fuels using the Area 3 High Sheer Rig Pratt & Whitney swirler and air blast atomizer,
- facilitate travel for University of Cape Town student,
- and advise the program Steering Committee.

Task #1: Integration and Coordination of NJFCP Teams

University of Dayton

Objective(s)

The objective of this task is to integrate and coordinate all ASCENT and non-ASCENT team efforts via facilitation of meetings, summarizing results, presenting results external to the NJFCP, communicating on a regular basis with the Steering Committee, and other related activities.



Research Approach

The NJFCP is integrated and coordinate via two main techniques: 1) the structural lumping of various teams into 6 Topic areas and 2) routine meeting and discussion both internal and external to individual Topic areas. The Topic areas are distinguished by the dominant physics associated with them (Topics I and IV), the culmination of all relevant combustion physics (Topics II, III, V), and wrapping all work into a singular OEM GUI package (Topic VI). These 6 Topic areas are:

Topic I. Chemical Kinetics: Foundational to any combustion model is a chemical kinetic model and the validation data anchoring modeling predictions.

Topic II. Lean Blow Off (LBO): This Topic covers data, screening, and validation at relevant conditions to statistically and theoretically anticipate fuel property effects on this FOM.

Topic III. Ignition: Similar to the LBO topic, the focus here is experimental screening and validation data for statistical and theoretical predictions.

Topic IV. Sprays: Historically, the dominant effect of fuel FOM behavior has been the spray character of the fuel relative to others. Experimentalists in this Topic area focus on measuring the fuel property effects on spray behavior. In analogy to Topic I, the spray behavior is not a FOM like Topic II and III, although it is critical to bound the physical property effects on combustion behavior relative to other processes, i.e. chemical kinetics.

Topic V. Computational Fluid Dynamics (CFD) Modeling: Complementary to the empirical Topics II, III, and IV, the CFD Modeling Topic focuses on the theoretical prediction of measured data and facilitates the development of theoretical modeling approaches.

Topic VI. User Defined Function (UDF) Development: Once the theoretical modeling approaches matured in Topic V are validated. UDFs are developed for OEM evaluation of fuel performance in proprietary rigs.

These topic area teams meet and coordinate on a regular basis. At minimum, NJFCP wide meetings are held monthly with Topic area meetings occurring typically every 2-3 weeks.

Milestone(s)

NJFCP Mid-Year Meeting 2017

NJFCP Year-End Meeting 2017, in preparation.

Major Accomplishments

Presentations at CRC Aviation Meeting, AIAA SciTech Meeting Paper and Presentation, NJFCP December 2016 and June 2017 meetings, JetScreen kick-off meeting, and ASCENT Spring and Fall presentations 2017.

Publications

Peer-Reviewed Journal Publications:

Colket, Meredith B., Joshua S. Heyne, Mark Rumizen, James T. Edwards, Mohan Gupta, William M. Roquemore, Jeffrey P. Moder, Julian M. Tishkoff, and Chiping Li. 2017. "An Overview of the National Jet Fuels Combustion Program." AIAA Journal, <https://doi.org/10.2514/1.J055361>.

Published conference proceedings:

Heyne, Joshua S., Colket, Meredith B., , Rumizen, Mark, Edwards, James T., Gupta, Mohan, Roquemore, William M., Moder, Jeffrey P., and Li, Chiping. 2017. "Year 2 of the National Jet Fuels Combustion Program: Moving Towards a Streamlined Alternative Jet Fuels Qualification and Certification Process. Grapevine, TX: American Institute of Aeronautics and Astronautics. (AIAA 2017-0145) <https://doi.org/10.2514/6.2017-0145>.

Outreach Efforts

Presentations at CRC Aviation Meeting, AIAA SciTech Meeting Paper and Presentation, ASCENT Spring and Fall presentations 2017, and DESS ASME conference.

Awards

Jeremy Carson – Best presentation DESS 2016, Best presentation DCASS 2017.

Student Involvement

Jeremy Carson, Graduate Research Assistant, January 2015 – May 2017 (graduated), now at UDRI.
Erin Peiffer, Graduate Research Assistant, June 2017 - present.

Jennifer Colborn, Undergraduate Research Assistant, August 2016 – August 2017, now at UDRI.
Katherine Opacich, Undergraduate Research Assistant, November – 2017 – present.

Plans for Next Period

Continue to perform all relevant coordination and integration related tasks, .

Task #2: Testing of NJFCP in a Well-Stirred Reactor

University of Dayton

Objective(s)

We aim to measure the Lean Blowout (LBO) limit and emissions/speciation characteristics for NJFCP fuels within the program.

Research Approach

In response to legislative orders, industrial and governmental organizations are actively pursuing strategies to promote alternative energy fuels in gas turbine combustors, and to reduce pollutant emissions. Emissions tend to be of importance because of the adverse effects they have on air quality, health and the environment. Gaseous emissions of interest include nitrogen oxides (NO and NO₂), sulfur oxides (SO_x), carbon monoxide (CO), carbon dioxide (CO₂) and unburned hydrocarbons (UHC). The International Civil Aviation Organization (ICAO) currently regulates the total amount of UHC among NO_x, CO, and particulate (smoke number) emissions for aircraft, but the concentration of these emissions, whether unburned hydrocarbons or carbon monoxide, etc., have been seen to have a local effect on areas around airports or flight lines (Anneken et al. 2014; D. L. Blunck et al. 2015; FAA 2012; Colket et al. 2016). Because of these effects and these initiatives, it is important to understand the emissions footprints of fuels for aviation for not only a sustainable future, but for better aircraft performance towards a carbon neutral future.

The National Jet Fuels Combustion Program (NJFCP) aims in streamlining the alternative jet fuel research and evaluation process, which is a major R&D directive covered in the Federal Alternative Jet Fuels Research and Development Strategy (AJF-IWG 2016; Colket et al. 2016). Use of specialized laboratory scale rigs are used in this program to determine fuel performance of a candidate alternative jet fuel while minimizing the use of multiple combustor rig tests. These rigs evaluate the impact of engine operability Figures of Merit (FOMs) such as lean blow off (LBO, high altitude relight, and cold start. These FOMs chosen indicate a strong impact on aircraft safety or engine hardware and are likely due fuel variation, whether due to the physical or chemical effects of the fuel. Performance and operability are also studied via emissions, combustor fuel coking and effects of temperature through pattern factors, radiation, and flame structure, all of which are secondary FOMs (Colket et al. 2016). It is imperative to investigate and pursue novel strategies and balance the combustor design characteristics with emissions reduction. Understanding performance and emissions with varying fuel composition provides the opportunity for use of potential alternative fuels in legacy and future aircraft and guidance to the quality and quantity of aircraft emissions produced.

Well-Stirred Reactor (WSR) experiments provide a simplified combustion environment to investigate chemical kinetic effects, among other parameters, such as combustion efficiency and LBO in the absence of physical property effects from the fuels. The lean premixed, prevaporized fuel and air mixtures used in these experiments remove physical effects such as droplet injection, evaporation, and atomization in addition to molecular mixing and transient and chemistry interaction of which is seen in typical gas-turbine combustors. With removing these physical effects, we also eliminate the physical complications native to modeling practical diffusion flame combustors such as, multi-dimensional flow, multi-phase fuel, and transient fluid dynamic and chemistry interactions. Use of this fundamental combustor experiment provides insight into LBO and emissions, a primary and secondary FOM in the NJFCP program, respectively, under relevant residence times and temperatures typically seen in practical gas-turbine-combustor environments (Colket et al. 2016).

We report the investigation of emissions and LBO of surrogate, conventional, and alternative fuel mixtures as lean combustion limits are approached in the WSR as funded by the FAA in relation to the NJFCP. The WSR has provided considerable

knowledge toward understanding lean and rich blow off limits, pollutant and particulate formation, kinetics of gaseous and liquid fuel combustion and combustion stability (D. Blunck et al. 2012; J. Blust, Ballal, and Sturgess 1997; S. D. Stouffer et al. 2005; J. W. Blust, Ballal, and Sturgess 1999; S. Stouffer et al. 2002; Manzello et al. 2007; Vijlee 2014; Scott Stouffer et al. 2007; Nenniger et al. 1984; Zelina 1995; Karalus 2013; D. L. Blunck et al. 2015). Knowledge of the emissions and LBO provides the opportunity to investigate the controlling chemical kinetics and relating chemical properties among the fuels. Here we report a statistically significant correlation between LBO, derived cetane number, and radical index, yielding insight to the controlling chemical effects experienced in typical gas turbine combustors near LBO.

I. Experimental Details and Methodology

Well-Stirred Reactor

LBO and emissions experiments were performed in the well-stirred reactor (WSR) facility at the Air Force Research Laboratory in Dayton, OH. The toroidal WSR design was derived from the work of Nenniger et al. (Nenniger et al. 1984), Zelina (Zelina 1995), and Stouffer (S. Stouffer et al. 2002) and approximates a zero-dimensional perfectly stirred reactor, *i.e.*, homogeneous in both space and time. The reactor, shown during operation in Fig. 1 a and b, comprises an Inconel jet ring, upper and lower ceramic reactor hemispheres, flow straightener, and exhaust stack. A representative cross section drawing of the reactor is shown in Fig. 1b. Premixed prevaporized fuel and air enter the jet ring through two opposed inlets to ensure equal flow around the reactor.

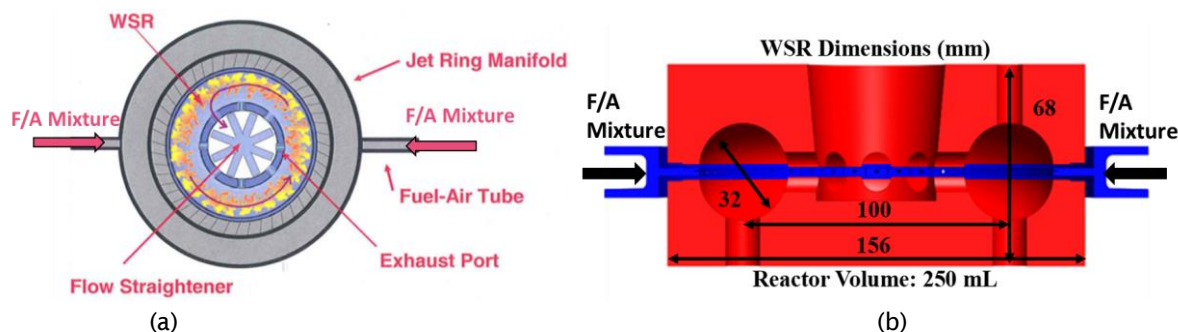


Figure 1. (a) Cross-section of the WSR, top view (S. D. Stouffer et al. 2005; Scott Stouffer et al. 2007). Premixed, prevaporized fuel and air enters the jet ring via the two opposed inlets. The angled jets (20 degrees from the radius of the torus) inject the mixture into the reactor, where bulk recirculation and flow occurs around the reactor. Burned products exit towards the inner diameter of the toroid through the exhaust ports, the flow straightener, and exhaust stack. (b) Cross-section of the WSR, side view. Fuel and air enter the toroidal reactor through the jet ring in blue.

In the current work, a fused silica reactor (Rescor 750, SiO₂) was utilized and sealed using spring loaded sections. (S. Stouffer et al. 2002; D. Blunck et al. 2012) This reactor material was chosen due to its low thermal conductivity, resistance to thermal cracking from fast transients, and reduction in the active cooling necessary around the reactor yielding reduced heat loss. An Inconel jet ring with 48 fuel/air jets at 1mm diameter was sealed between the reactor components. A ceramic paper gasket seal (Cotronics 390, 1/8" thickness) was placed between the upper reactor halve and jet ring while a mica gasket (0.064" thickness) was placed between the jet ring and bottom half to seal the reactor under fuel-lean operating conditions. Figure 1 highlights the construction of the WSR with the ceramic components in red and the jet ring in blue.

The feed jets in the jet ring inject the premixed fuel/air at an angle 20 degrees off the radius of the torus causing the bulk flow to move circumferentially around the reactor (S. D. Stouffer et al. 2005; S. Stouffer et al. 2002; Vijlee 2014; Scott Stouffer et al. 2007; Nenniger et al. 1984). The sonic velocity and angle from the jets provides for recirculation zones around the upper and lower half of the toroid in addition to around the toroid. The high rate of continuous mixing between the unburned reactants and burned products is an additional characteristic that separates the WSR from other premixed combustions systems (Briones et al. 2008; D. L. Blunck et al. 2015; D. Blunck et al. 2012; S. D. Stouffer et al. 2005; Scott Stouffer et al. 2007). Previous work using numerical modeling has been performed to show that the WSR operates in the well-stirred turbulent regime (Briones et al. 2008). Products from combustion exit the reactor via 8 radial ports at the toroid inner diameter and through a 5-cm-diameter ceramic stack above the WSR. In this region, recirculation zones and bulk flow are reduced via the use of an alumina flow straightener, rested at the end of the exhaust and base of the stack (D. L. Blunck et al. 2015).



Liquid fuel is delivered to the vaporizer by two syringe pumps (Isco 500 D) operated in continuous flow mode. The piston flow meter accuracy is $\pm 0.5\%$. The liquid fuel passes through a swirler and enters a heat exchanger, where the fuel reaches a temperature of 473 K at the inlet of the vaporizer. Heated fuel is introduced in the vaporizer with 10-20% of the total combustion air via an air-swirled atomizer nozzle containing heated air at 400 K and mass flow of 60 standard liters per minute (slpm). Remaining air at 489 K and mass flow of 440 slpm is added in the vaporizer as a coaxial stream (Scott Stouffer et al. 2007). Prior to entering the vaporizer, the airlines are filtered and monitored along with being controlled using two mass flow controllers, one rated at 1000 slpm and one rated at 75 slpm (Brooks Instruments) (S Stouffer et al. 2002). The accuracy for the mass flow controllers is rated at $\pm 1\%$ full scale and a repeatability of 0.25% of the flow rate. The flow controllers were measured and calibrated using sonic nozzles to allow for a more accurate measurement of the air flow rate. Electric, PID-controlled heaters preheat the incoming fuel and air streams. Flow rates of the fuel and air, paired with the temperature control of each, are used to control the incoming fuel-air mixture to the reactor. These flow rates ensure turbulent mixing and sonic velocities from the jets into the reactor (Vijlee 2014). The vaporizer used for the atmospheric WSR has been used in previous tests and was shown to safely and successfully mix the fuel with the air (S. D. Stouffer et al. 2005; Scott Stouffer et al. 2007). This strategy, using premixed and pre-vaporized fuel, eliminated physical complications associated with droplet combustion and established an ideal premixed combustion environment without physical complication.

A fixed custom spark igniter within the reactor initiates combustion. When testing with liquid fuel, the reactor was first brought to a stable thermal condition using a gaseous fuel (usually ethylene). Gaseous fuel flowrate into the WSR was controlled with a series of pressure regulators, to slowly reduce pressure, and mass flow controllers (Brooks Instruments). Introducing gaseous fuel before the liquid fuel allowed the reactor to effectively preheat for prevention of fuel condensation within the small jet ring passages. After operational temperatures were reached, the fuel was transitioned smoothly from the gaseous fuel to the given liquid fuel (Scott Stouffer et al. 2007).

B. Fuels

Four fuels tested in the current work are part of the National Jet Fuels Combustion Program (NJFCP). The NJFCP focus is to streamline the certification process for alternative jet fuels. Here the focus is to study the fundamental fuel kinetics and investigate the impact of alternative fuels on engine operability FOMs relative to reference fuels (Colket et al. 2016), enabling the process to be streamlined. FOMs such as cold start, altitude relight and LBO are key parameters considered in these fuels studies (Colket et al. 2016). The WSR is aimed to focus on the LBO FOM of engine operability in addition to determining the emissions footprint of the fuels in similar gas turbine combustor environments. The test fuels and their properties are shown in Table 1. These test fuels were characterized from the Combustion Rules and Tools for the Characterization of Alternative Fuels (CRATCAF) program and defined previously by OEMs (Colket et al. 2016). The category A fuels are intended to represent current jet fuels over a range of properties seen in current practice. Previous work has shown that flash point, aromatic content, and viscosity are of most impact for combustion behavior (Colket et al. 2016). A-2 and A-3 are fuels which exhibit 'average'/'worst' physical and chemical properties such as flash point, viscosity, aromatics, density, and derived cetane number respectively, giving an expectation envelope for conventional fuel combustion properties as they map to combustion behavior. C-1 and C-5 are alternative test fuels down selected by the NJFCP committee in 2015 from a total of six alternative jet fuel solvents (Colket et al. 2016). These fuel blends were selected to have properties near or exceed the limits acceptable jet fuels (i.e. viscosity, distillation curve, and chemical composition) (Colket et al. 2016). C-1 is composed of highly branched iso-paraffinic molecules with 12 and 16 carbon atoms, which have a low reactivity as exhibited by a derived cetane number of 17.1 (Colket et al. 2016). C-5 is a test fuel composed of two components, an isoparaffinic 10 carbon molecule and 1,3,5 trimethyl-benzene, which results in a flat boiling temperature/distillation curve (Colket et al. 2016). These two test fuels, C-1 and C-5, were intended to investigate effects of low cetane and narrow vaporization range of fuels on these combustor FOMs (Colket et al. 2016).


Table 1. Properties of the NJFCP Fuels Used for Testing in the WSR.

Fuel ID	A-2	A-3	C-1	C-5
POSF	10325	10289	12368	12345
Empirical Formula	$C_{11.4}H_{22.1}$	$C_{11.9}H_{22.6}$	$C_{12.6}H_{27.2}$	$C_{9.7}H_{18.7}$
AMW (g/mole)*	159	166	178	135
H/C Ratio	1.939	1.899	2.159	1.928
Stoichiometric Fuel/Air	0.0685	0.0687	0.0671	0.0686
Heat of Combustion (MJ/kg)	43.3	43	43.9	42.8
Density (g/cc)**	0.803	0.827	0.759	0.770
Derived Cetane Number (DCN)***	48.3	48.8	17.1	39.6

*Average molecular weight (AMW) measured using GCxGC

**Density measured using ASTM 4052, 15°C (kg/L)

***DCN measured using ASTM D5890(Colket et al. 2016)

Additional fuel surrogates were studied to investigate the effects of chemical structure on combustion performance and emissions and compared against current conventional fuels and fuel solvents. The surrogate fuels were chosen from the Strategic Environmental Research and Development Program (SERDP) aimed at studying the science of emissions of alternative fuels. *n*-Dodecane was used as a base fuel, and commonly used as a second generation fuel surrogate, emulating JP-8 flame speed. This surrogate provides a better representation of the *n*-alkane content in jet fuels. *m*-Xylene was chosen as an additive to the base surrogate fuel to study the effects of aromatic content, and was chosen as 25% by volume to emulate the aromatic limit of JP-8. Molar carbon for the additive was kept constant to the aromatic content in the *n*-dodecane mixture, establishing a baseline for comparing surrogate performance. This fuel surrogate represents the *iso*-alkane hydrocarbon structure in jet fuels, and typically found in gas-to-liquid and FT fuels. Methylcyclohexane is used as the fuel surrogate for the cycloparaffins found in coal derived fuels. *n*-heptane is a straight chained hydrocarbon that mimics the light hydrocarbons in jet fuel and represents straight chain alkanes for a gasoline fuel surrogate. All surrogate mixtures in this paper were formulated to preserve the same carbon mole fraction as the *m*-xylene additive. Table 2 contains a list of relevant fuel properties pertaining to the WSR. Derived cetane number (DCN) for S-1, S-2, S-4, and S-5 were measured using the same ASTM standard as the NJFCP fuels. The DCN for S-3 was calculated using the summation of the volume fraction of the given fuel multiplied by its corresponding cetane number(Yanowitz et al. 2004).



Table 2. Properties of the Surrogate Fuels Used for Testing in the WSR.

Surrogate Blends	<i>n</i> -dodecane (61.8 mol%) / <i>m</i> -Xylene (38.2 mol%)	<i>n</i> -dodecane (61.8 mol %) / <i>iso</i> -Octane (38.2 mol%)	<i>n</i> -dodecane	<i>n</i> -dodecane (58.6 mol%) / Methyl-cyclohexane (41.4 mol%)	<i>n</i> -dodecane (58.6 mol%) / <i>n</i> -heptane (41.4 mol%)
Fuel ID	S-1	S-2	S-3	S-4	S-5
Empirical Formula	C _{10.47} H _{19.9}	C _{10.49} H _{22.98}	C ₁₂ H ₂₆	C _{9.93} H _{21.03}	C _{9.93} H _{21.86}
H/C Ratio	1.900	2.191	2.167	2.118	2.201
Stoichiometric Fuel/air	0.0687	0.0669	0.0670	0.0673	0.0668
MW	145.84	149.12	170.31	140.45	141.28
Density (g/cc)	0.778	0.737	0.750	0.758	0.734
Derived Cetane* Number (DCN)	57.47	60.91	78.5	54.05	67.46

*DCN for S-1, S-2, S-4, S-5 measured using ASTM D5890(Colket et al. 2016)

C. Emissions and Instrumentation

A bare, linear-tracking, custom, type-B thermocouple (0.2mm diameter, platinum – 6% rhodium, platinum – 30% rhodium) without coating was used to measure reactor temperature. Measurements for temperature were taken at 0.25" from the outer wall of the reactor and were not corrected for radiation and other heat losses. Therefore, the gas temperature readings may not be accurate in an absolute sense, yielding lower temperatures than expected, but enable relative comparisons between conditions. The thermocouple location is within the uniform temperature region in the WSR and the temperature can therefore be taken as the average temperature in the reactor. A 0-5 psia pressure transducer was used to monitor the slight pressure increase in the reactor during operation. A maximum pressure of 5.5 kPa above ambient conditions was experienced during testing.

Exhaust samples were extracted using an oil-cooled probe (420 K) through a 1.4-mm-diameter orifice. The samples were passed through the probe which quenches the reactions, similar to quenching in a typical combustor (D. Blunck et al. 2012). The probe rested 5 mm above the wall of the lower toroid and is 90 degrees around the axis of the toroid from the thermocouple. Temperatures of the oil were kept constant at 420 K while sampling to minimize condensation in the sampling line.

Gaseous emissions were transported through a heated line containing a pump, filter and oven before entering the Fourier Transform Infrared (FTIR) analyzer. The heated lines and oven were maintained at 420 K by PID controllers. Flow entered and exited the FTIR at a constant temperature of 463 K where it was exhausted or sampled via charcoal tubes and gas bags. A sketch of the sampling methodology is shown in Fig. 3.

The FTIR system utilized in the current work was a MKS 2030 High Speed (5Hz) gas analyzer with a gas cell path length of 5.11 m and was used to measure the emissions from the WSR. This FTIR system allows major gaseous species to be detected online, while saving the spectra for later detailed investigation. The Gasoline Ethanol method, within the MKS software package, was employed to analyze the IR spectra and calculate emission concentration values. Measurement accuracy using this FTIR is +/- 2%. Carbon monoxide (CO), carbon dioxide (CO₂), water (H₂O), nitrogen oxide (NO), nitrogen dioxide (NO₂), acetylene (C₂H₂), ethylene (C₂H₄), and formaldehyde (CH₂O) are among the many emissions that absorb infrared radiation and can be quantified using the method employed in the FTIR.

Following the FTIR was a valve to capture bag samples and enable offline measurement of C1–C12 species, primarily for C1–C4 hydrocarbons. An Agilent 6890/5973 GC-FID-MS (Gas Chromatography-Flame Ionization Detector-Mass Spectrometry) and Gas Pro Column was utilized to analyze emissions from the extracted samples. Capturing exhaust emissions through charcoal tubes was also employed as a sampling technique to obtain heavy hydrocarbon species, generally above C4 species.

Another valve following the FTIR was used to draw these samples. A pump drew 1-liter exhaust emission samples at a rate of 1 liter per minute. Remaining gases pulled through the pump were exhausted through the hood where the WSR operates. Previous work has been performed using this method to extract hydrocarbons from jet-fuel emissions (Anneken et al. 2014). The tube was later extracted with carbon disulfide and the mass of each component was measured using an Agilent 7890 GC-FID and Gas Pro Column.

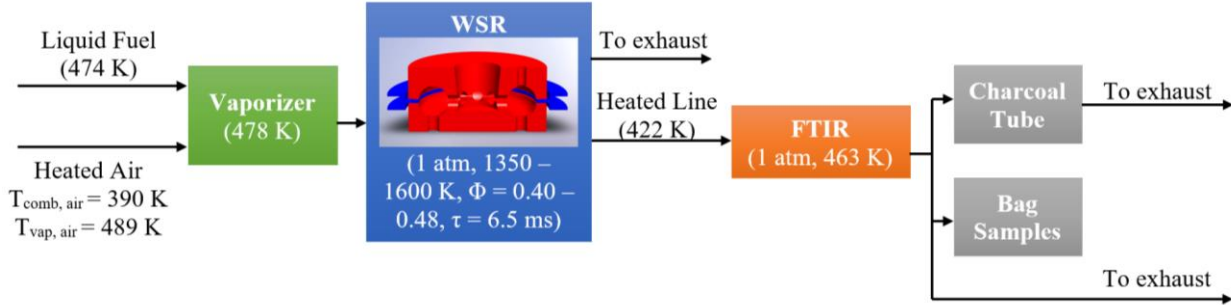


Figure 2. Experimental Schematic for WSR Emission Studies. A heated line takes the sample from the reaction region in the WSR to the FTIR. Charcoal tube and bag samples are taken after the FTIR before being exhausted.

During testing, online concentration measurements of various species were made using an FTIR. Roughly 95% of the carbon containing species were recovered by the FTIR at the higher equivalence ratios, reducing to roughly 92% near LBO as shown in Figure 3. The ~5% carbon deficit can be attributed primarily to FTIR measurement uncertainties. In addition, insufficient quenching during extractive sampling from the WSR can contribute to the uncertainty as sampled could react in the sampling lines and measurements are not representative of the actual combusting environment. The high percent of carbon recovered provides confidence as to the quantitative fidelity of species measured and the relative species concentration between fuels.

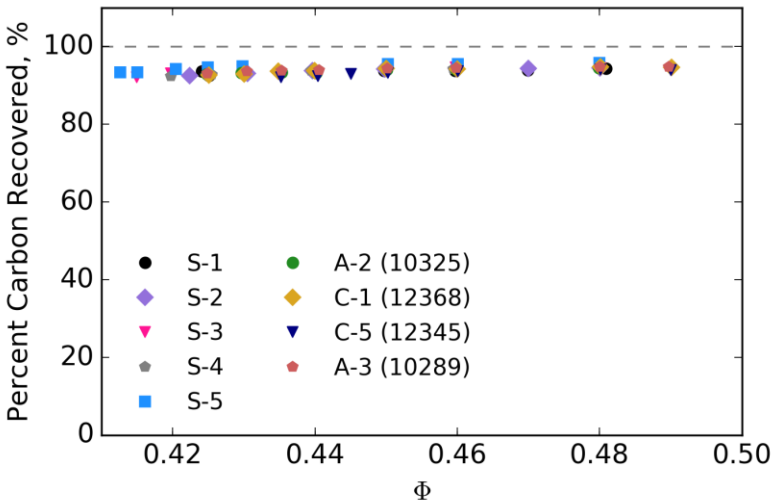


Figure 3. Carbon recovery from the species captured via online FTIR sampling. A decrease in percent carbon recovered is seen as equivalence ratio (Φ) is decreased. This signifies that intermediate species are produced and some are not recovered using this emissions measurement technique. The high percentage of carbon recovered provides confidence that this method captures emissions adequately to yield quantitative results.

II. Experimental Conditions

The equivalence ratio was set by varying fuel flow rate. Each LBO measurement was initiated at an equivalence ratio of >0.48 where formaldehyde levels dropped below the detection limit (≈ 0 ppm). Equivalence ratios were reduced by keeping air constant and decreasing fuel flow until LBO where the flame extinguished. Heat loss at LBO conditions becomes too large and combustion is unstable and is not sustained. A drop in reactor temperature and change in noise generated by the reactor corresponded to a LBO (Scott Stouffer et al. 2007).

Temperatures at these conditions were well below the maximum operating temperature of the ceramic. This enabled durability for testing with a single build of the reactor and prevented cracking. Premixed fuel and air coming into the jet ring was held at a constant temperature of 460 K, which is in the typical combustor range of 200–900 K (McAllister, Chen, and Fernandez-Pello 2011; Colket et al. 2016). Reactor temperatures during the test varied between 1350 K and 1500 K based on the heat of combustion of each fuel and heat loss from the system. The heat loss from the system was estimated at 5% using the ceramic reactor (J. Blust, Ballal, and Sturgess 1997). The health of the ceramic reactor was monitored by measuring the temperature of the jet ring. When a crack formed, a large asymmetric temperature profile was observed in the jet ring. Towards leaner conditions, the jet ring temperature profile varied a maximum of approximately 2% (10 K) peak-to-peak, indicating the ceramic reactor remained free from cracks.

Global reacting residence time for the experiments was 6–7 ms. Bulk residence time was calculated using the volume of the reactor, the flow rates of the fuel and air, and the density of the mixture under reacting conditions. Variations in residence time were primarily a result of changes in reactor temperature and fuel mass flow since change in reactor pressure and molecular weight are small (Scott Stouffer et al. 2007). At most points throughout each experiment, the reactor was allowed to reach a thermal steady state and then held at constant flow and thermal conditions for more than 12 minutes. Non-emission data was captured from a running average of approximately 12 seconds every 3 minutes.

FTIR measurements, recorded continuously at 5 Hz, were averaged over the 12 second running average period for each sample, while gas bags and charcoal tubes were taken at the last point of the sampling process for each equivalence ratio. This holistic sampling process captured major and minor species throughout the duration of the experiment, while ensuring steady state conditions for the bag and charcoal tube samples.

For points at or near LBO, the reactor could not be held constant for 12 minutes because of the tendency to blow off. At these near-LBO conditions, a non-steady-state condition between the wall and gas temperatures may be responsible for some scatter in the WSR temperature data. Once blow off occurred, the reactor was re-ignited by reducing air and fuel flow rates. Once steady state conditions were reached at the start of the blow off test, a second test was conducted in a similar fashion. As experienced in previous experiments, hysteresis does exist in approaching LBO if there is insufficient time for the reactor to reach a steady-state temperature at each condition. Leaner conditions can be reached if the reactor walls are relatively hot, resulting from a rapid decrease in equivalence ratio. If LBO is approached more slowly, the walls have sufficient time to cool to the local gas temperature and, therefore, LBO is experienced at higher equivalence ratios (Vijlee 2014). Increments were small while decreasing the fuel flow, thus reducing the chance for hysteresis. Previous literature showed variance in blow off temperature of ± 50 K (Vijlee 2014) and uncertainty of blow off equivalence ratio near 2% (D. L. Blunck et al. 2015). Based on the sonic nozzle calibration and the self-consistency between the two or more LBO tests per fuel, the uncertainty in equivalence ratio was estimated as $\Phi \pm 0.0025$. The primary parameter controlling the uncertainty was the repeatability of the air mass flow controllers based on the operating conditions.

Table 3. Operating conditions using the WSR

Pressure (atm)	1
Inlet Temperature (K)	460
Reactor Temperature (K)	1350 – 1600
Bulk Residence Time (ms)	6 – 7
Mass Flow Air (g/min)	600
Equivalence Ratio	0.425 – 0.49

III. Results and Discussion

D. LBO

LBO occurs when the flame cannot be sustained because of either fluid dynamic or chemical processes. In the WSR, LBO is most sensitive to chemical processes associated with heat release, and ideally insensitive to mixing and fluid processes. Experimental results are shown in the figures below for the four NJFCP fuels and the five surrogate mixtures. Figure 4 shows the effect of lowering the fuel flow, hence lowering the equivalence ratio. The reactor trends to decrease linearly with leaner conditions. C-1 shows to have the least resistance to LBO, having the highest Φ at LBO, while the S-3 and S-5 straight chained alkane surrogates trended to have the most resistance to LBO. LBO occurs at the lowest recorded equivalence ratio of roughly 0.414. In contrast, the C-1 fuel exhibits LBO at the highest recorded equivalence ratio.

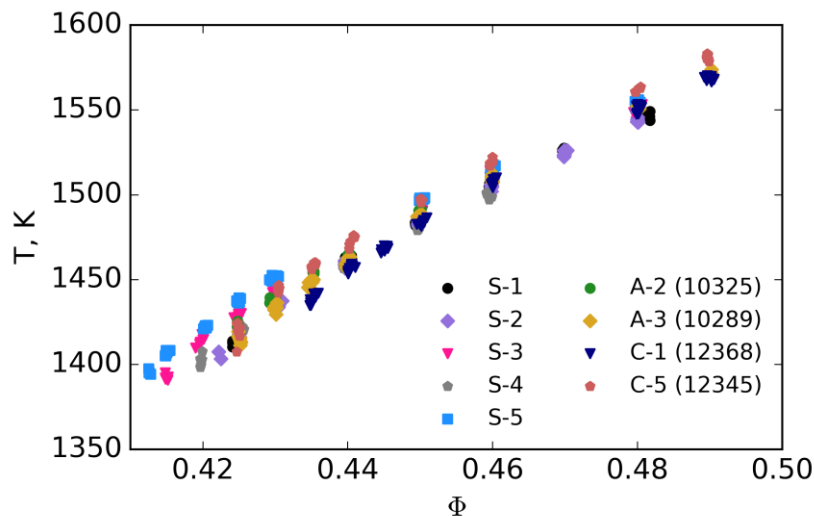


Figure 4. Reactor temperature (K) as a function of Φ for the fuels. Points represent the samples taken at each equivalence ratio tested. As leaner conditions are approached, the reactor temperature lowers linearly to the point where combustion cannot be sustained, corresponding to LBO. C-1 has the least resistance to LBO, having the highest Φ at LBO, while S-3 and S-5, straight chain alkane blends, trended to have the most resistance to LBO.

Since the WSR is operating in a lean, premixed, prevaporized combustion environment, the combustion property targets (CPTs) can be investigated as it relates to LBO. These CPTs, H/C ratio, MW, Threshold Sooting Index (TSI), and derived cetane number (DCN), have shown to sufficiently match combustion behaviors in pre-vaporized environments for petroleum-derived and synthetic jet fuels (Won, Veloo, Santner, Ju, Dryer, et al., n.d.). H/C ratio is used as it relates energy density of a particular fuel, as well as describes the composition and the distribution of radicals produced from combustion processes. (Won, Veloo, Santner, Ju, Dryer, et al., n.d.) LBO is shown below in Figure 7 as a function of H/C ratio. For each fuel, the last sampled condition immediately preceding LBO was averaged for both runs. If LBO occurred during sampling, the mean LBO was calculated using the average of those samples with the previous full sample preceding LBO. The uncertainty bars represent the uncertainty based on the air and mass flow rates. Towards the left of Fig. 5, mean LBO was nearly identical at ~ 0.425 . This is a result of the roughly 0.005 ($\sim 1\%$) step size in equivalence ratio, used to obtain stable points for emissions capture near LBO. The mean Φ represents roughly the last point captured for emissions data before blow off occurs. However, based on the given fuels and their LBO conditions, there exists a distribution of fuels which lie outside the bounds of the uncertainty estimated and are statistically significant. Based on the current distribution of data, there doesn't exist a correlation of LBO for the given fuels with varying H/C ratios. Molecular weight was also plotted as a function of Φ for the fuels. This property corresponds to the reactivity of the fuel via the normal and branched alkanes in the fuel and also does not trend to correlate, shown in Figure 6.

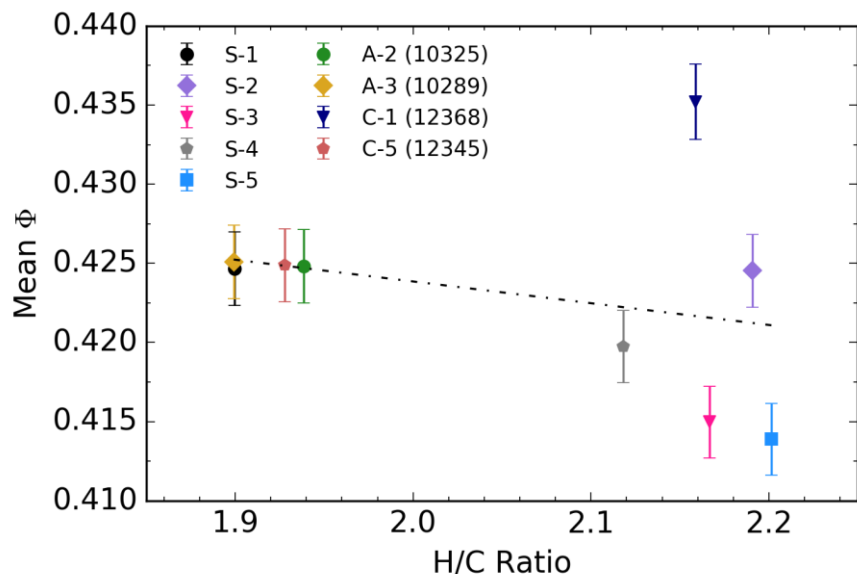


Figure 5. Mean Φ as a function of H/C Ratio. Points represent the average of the data at each equivalence ratio, while the error bars represent the uncertainty of the measured and averaged Φ . (Eq. $-0.01374x + 0.45134 = y$, $R^2 = 0.0849$).

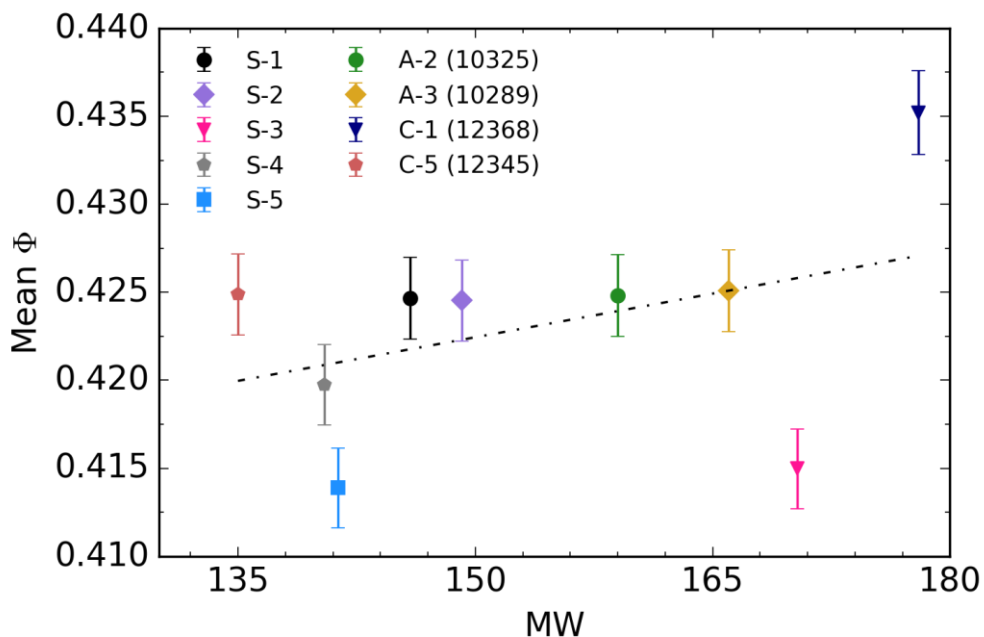


Figure 6. Mean Φ as a function of molecular weight. Points represent the average of the data at each equivalence ratio, while the error bars represent the uncertainty of the measured and averaged Φ . (Eq. $1.652E-04x + 0.3977 = y$, $R^2 = 0.1527$).

TSI, another CPT, correlates the competition of aromatic molecules and highly-branched alkanes with the radical pool and is important as it describes the sooting tendency of a fuel (Won, Veloo, Santner, Ju, Dryer, et al., n.d.). This correlation of reactivity of a fuel varies inversely with TSI, using this methodology (Won, Veloo, Santner, Ju, Dryer, et al., n.d.). Values were

estimated for the given surrogate fuels using linear combination of each mole percent of components by their corresponding TSI. (Mensch 2009) Based on Fig. 9 below, there doesn't exist to show a correlation among the TSI and LBO. Although there is no apparent correlation, the effect of aromatic content in S-1 shows to have an effect on increasing the TSI, where further investigation on determining the TSI of the conventional and alternative fuels would be useful.

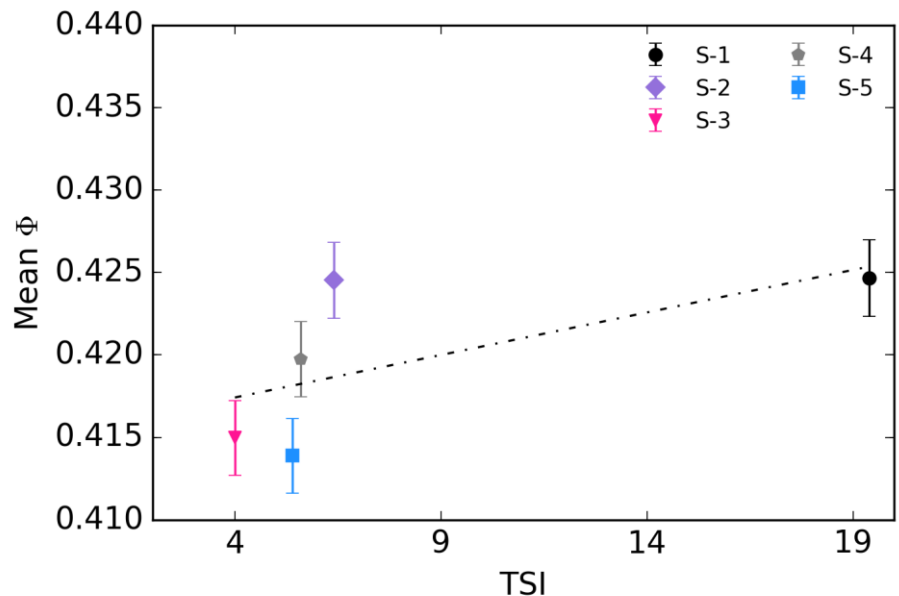


Figure 7. Mean Φ as a function of TSI. Points represent the average of the data at each equivalence ratio, while the error bars represent the uncertainty of the measured and averaged Φ . (Eq. $5.158E-04x+0.41536= y$, $R^2 = 0.41134$).

Figures 8 and 9 display the effects of LBO with DCN and radical index, respectively. Based on the given data set and Fig. 8 below, there appears to be a functional dependence on cetane number of the fuel when comparing to LBO. Low derived cetane numbers correspond to a longer ignition delay, which is a potential attribute to the LBO difference seen in the given fuels set. This trend can yield understand towards this parameter and potential implications in gas turbine combustors. Also, the tested data only contains two emissions profiles per fuel, yielding some additional uncertainty.

Radical indices were approximated from literature (Won, Veloo, Santner, Ju, and Dryer, n.d.; Won, Dooley, et al., n.d.). S-1 and S-2 were estimated using the radical indices of the surrogate mixture components multiplied by the corresponding mole percentage. The radical index for *m*-xylene was approximated between toluene and 135TMB assuming a linear correlation (Won, Dooley, et al., n.d.). S-3 and S-5 mixture was approximated at 1, being of n-paraffinic structure, where A-2 and C-1 were assumed to be similar to JP-8 and IPK, respectively (Won, Veloo, Santner, Ju, and Dryer, n.d.). A-3 was assumed to be of JP8 (Won, Veloo, Santner, Ju, and Dryer, n.d.), even though A-3 contains more iso-paraffins. The radical indices for *iso*-octane and JP8 were near identical and used as a rough estimate to investigate potential correlations of LBO with radical index. A radical index for *m*-xylene was approximated between the values of toluene and 135TMB, assuming a linear relationship between the values. These preliminary approximations show a correlation with LBO as seen in Fig. 8. The higher radical index indicates a larger radical pool in which the radicals aid in sustaining combustion, tending to blow out at leaner conditions. Towards the left portion of Fig. 6, C-1 trends to blow out at a higher equivalence ratio, where it has the lowest assumed radical index. Behavior experienced in Figure 8 and 9 show a similar trend with LBO and indicate dependence on DCN and on radical index. This knowledge, along with the ability to create surrogates to vary one of the characteristics (DCN or RI), can assist in further understanding the extinction and LBO behavior of a given fuel.

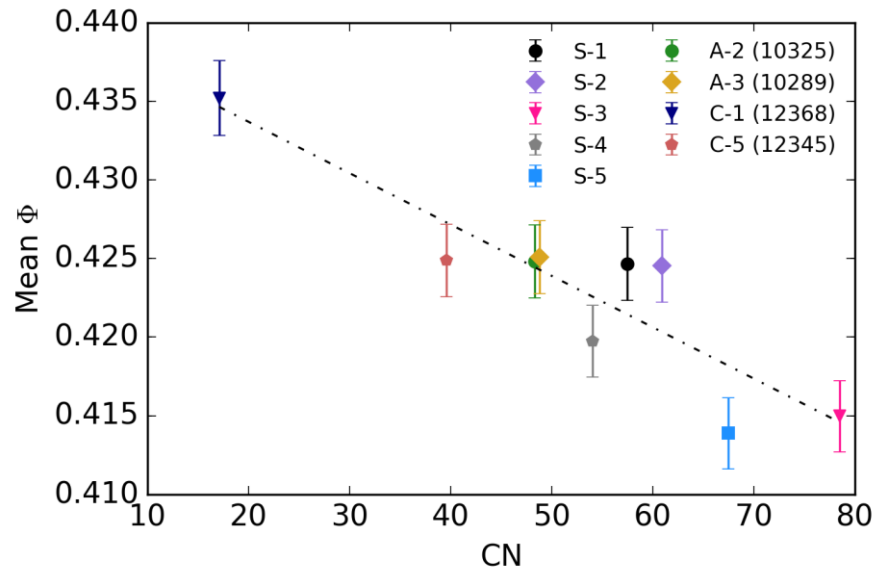


Figure 8. Mean Φ as a function of DCN. Points represent the average of the data at each equivalence ratio, while the error bars represent the uncertainty of the measured and averaged Φ . (Eq. $-3.268E-4x + 0.44023 = y$, $R^2 = 0.8097$). Percent Difference in Φ from S-5 to C-1 is ~5%.

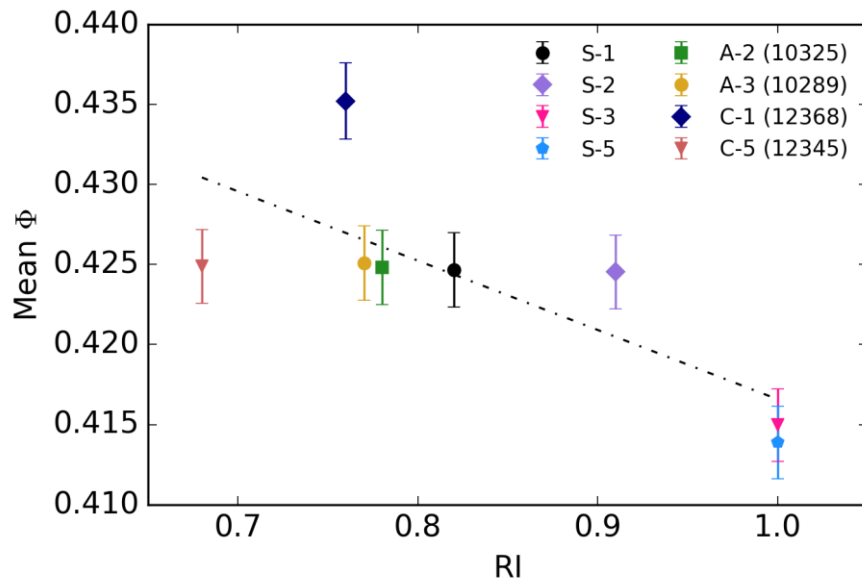


Figure 9. Mean Φ as a function of Radical Index. Points represent the average of the data at each equivalence ratio, while the error bars represent the uncertainty of the measured and averaged Φ . (Eq. $-0.04328x + 0.4599 = y$, $R^2 = 0.585$)

E. Emissions Profile

As described in the previous section, the fuel chemistry can play an important role in LBO. For instance, surrogate fuels may have a similar heat of combustion and derived cetane number, S-1 and S-2, but different radical index, 0.82 and 0.91 respectively. This difference in radical index can be caused by the presence of radical-promoting reactions and/or radical-trapping reactions that occur as a result of the fuel chemistry, in this case aromatic or iso-alkane content. The WSR is specifically designed to provide relevant information on the effects of fuel chemistry on combustion emissions and stability

under conditions similar to those in typical combustors, specifically the primary and secondary zones. This approach enables fuel-specific emissions fingerprints to be generated while approaching LBO. The species produced under these conditions are highly sensitive to the specific fuel chemistry and, therefore, provide a sensitive metric for developing reduced-order chemical mechanisms. These emissions profiles can also be utilized along with the DCN, radical index, H/C ratio, MW, and TSI to determine the chemical property dependencies driving LBO in various experimental arrangements.

Figure 10 shows the major carbon-containing combustion products, as a function of equivalence ratio, produced during testing of the WSR. CO and CO₂ compose approximately 99.9% and 99% of the total carbon count in the sampled emissions at the areas of higher equivalence ratios and towards the leanest conditions, respectively. As the fuel rate decreases to leaner conditions, less CO₂ is produced allowing for intermediate species to be formed as a result of incomplete combustion and thus incomplete conversion to CO₂. As observed in Figure 10(a), CO₂ produced from the C-1 fuel and the S-2 surrogate mixture are similar yet follow a distinctly different curve towards LBO relative to the other fuels, although C-1 LBO occurs at a higher equivalence ratio. In contrast, CO is increased as LBO is approached for all fuels. The two bounding fuels are S-5 which produced the most CO₂ and least CO and C-1 which produced the least CO₂ and most CO for a given equivalence ratio.

Although the carbon deficit in the CO₂ production between C-1 and S-5 was primarily recovered in the form of CO, the total carbon count for the six largest carbon containing species is shown in Figure 11. It is clear that at $\Phi = 0.435$, C-1 produces an order of magnitude more formaldehyde than any other fuel, in addition to increased concentrations of ethylene, acetylene, methane, and isobutene.

Formaldehyde production as a function of equivalence ratio is displayed in Figure 12 for all fuels. This species is particularly important as it is a key intermediate species in the oxidation of hydrocarbons and can significantly shorten the ignition delay time of fuel/air mixtures. Specifically, previous work has shown that many hydrocarbon species can be linearly related to formaldehyde production, regardless of fuel type (D. L. Blunck et al. 2015), although C-1 tends to be the outlier. Methane recorded from the FTIR is seen to exhibit that linear relationship as a function of formaldehyde, as observed in the same figure. For this reason, species production in all subsequent figures are plotted against both equivalence ratio and formaldehyde.

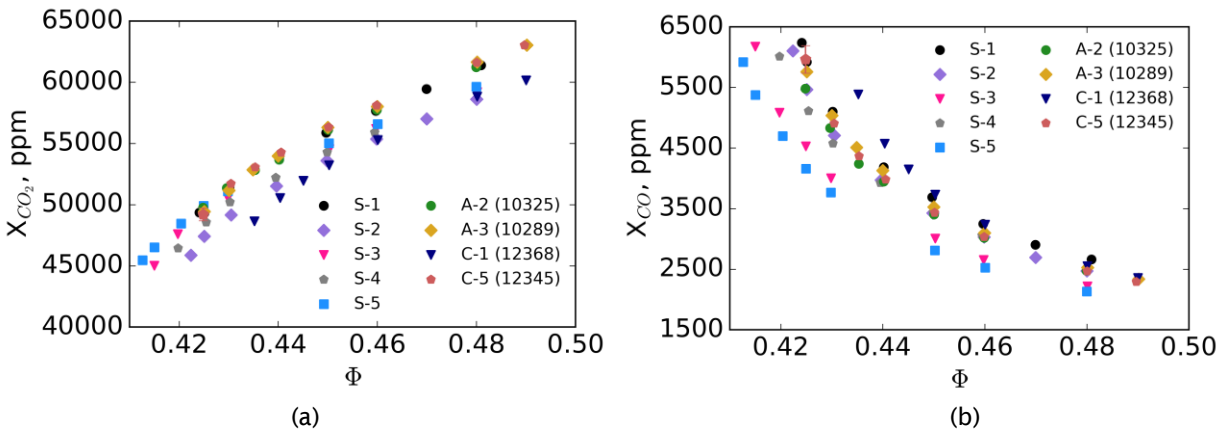


Figure 10. CO₂ (a) and CO (b) as a function of equivalence ratio (Φ). Points represent the average of the data at each equivalence ratio, while the error bars represent one standard deviation. Trends in decreasing CO₂ and increasing CO while approaching leaner conditions is expected, signifying losses in combustion efficiency towards LBO.

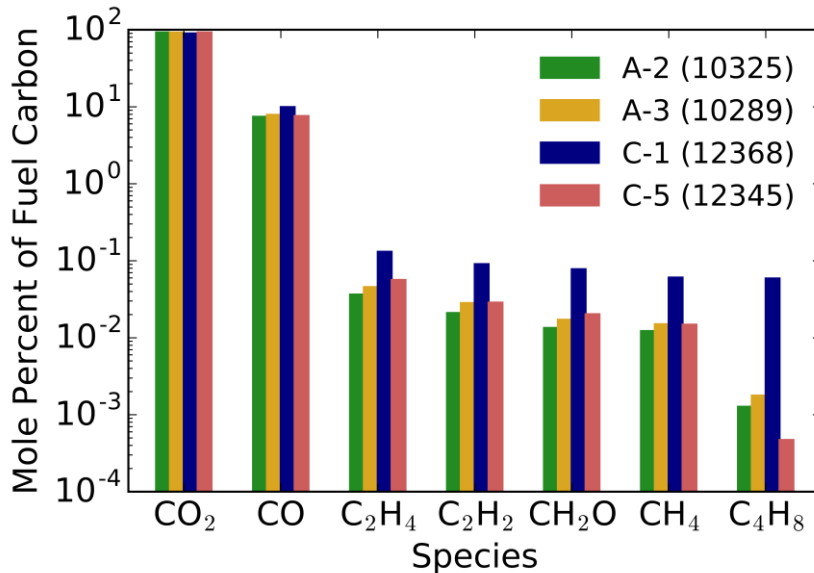


Figure 11. Mole percent of fuel carbon on the given species at $\Phi = 0.435$. C-1 appears to be most distinguished, as it is at the leanest condition before LBO, producing more intermediate species.

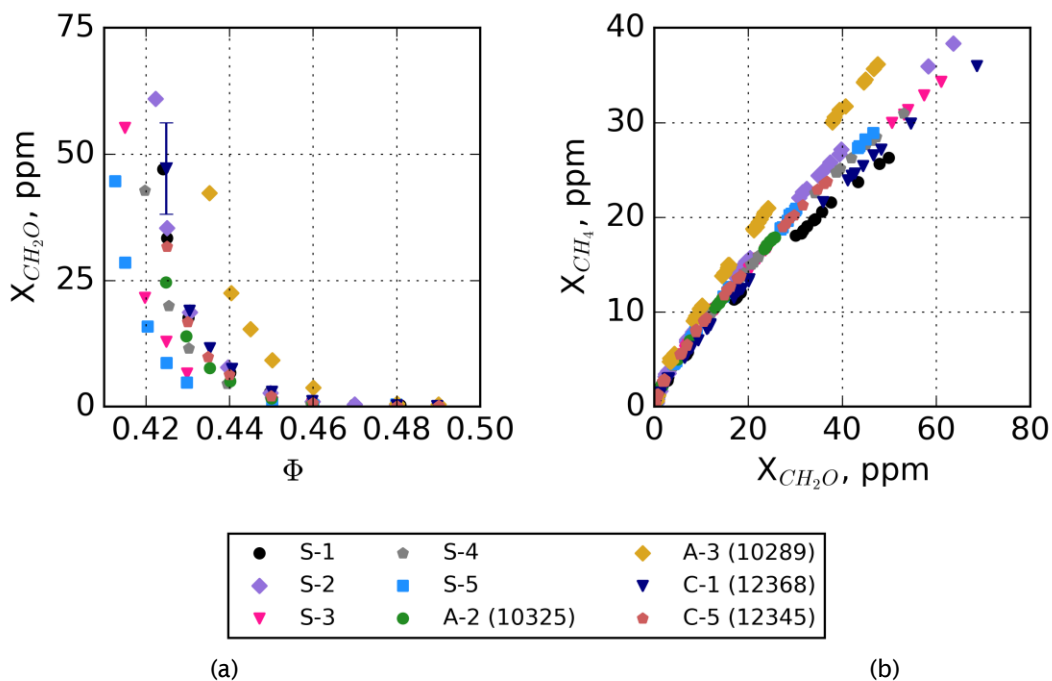


Figure 12. Formaldehyde (CH_2O) as a function of equivalence ratio (Φ) and methane (CH_4) as a function of formaldehyde production. Points represent the average of the data at each equivalence ratio, while the error bars represent the maximum standard deviation in the reported set.

Figure 13 and 14 displays ethylene and acetylene production towards lean low off conditions using the online FTIR method, respectively. Figures 17 and 18 show the isobutene production using both the FTIR and charcoal tube methodologies of capturing emissions.

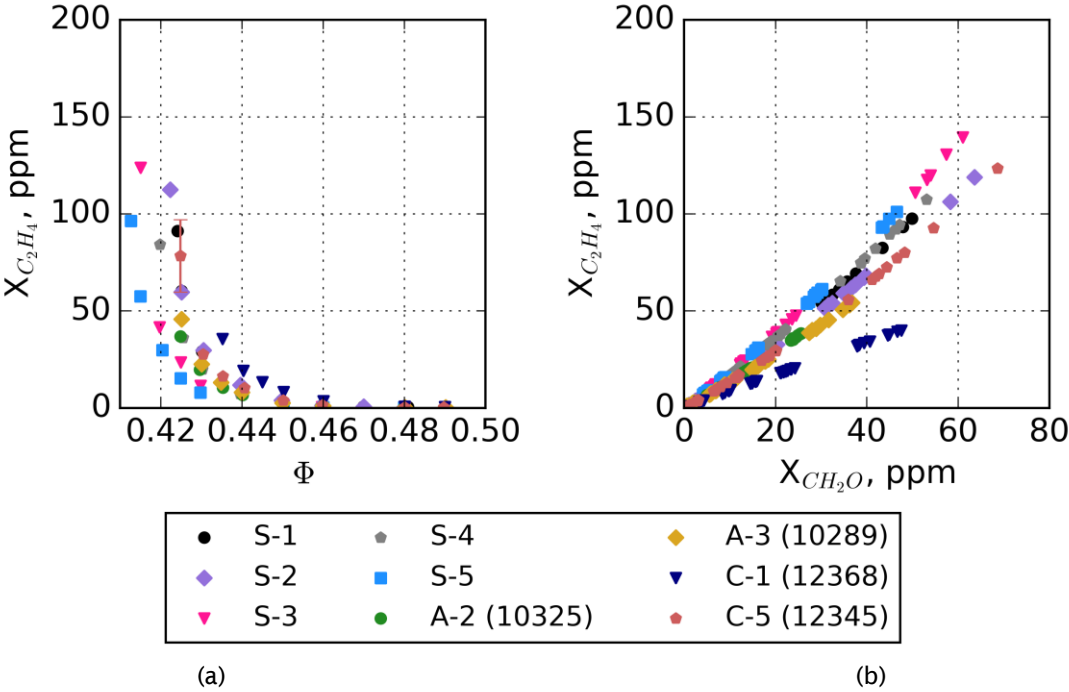


Figure 13. Ethylene (C_2H_4) as a function of equivalence ratio (Φ) sampled from the FTIR. (a) Points represent the average of the data at each equivalence ratio, while the error bars represent the maximum standard deviation in the reported set. (b) Points represent the all the sampled data as a function of formaldehyde.

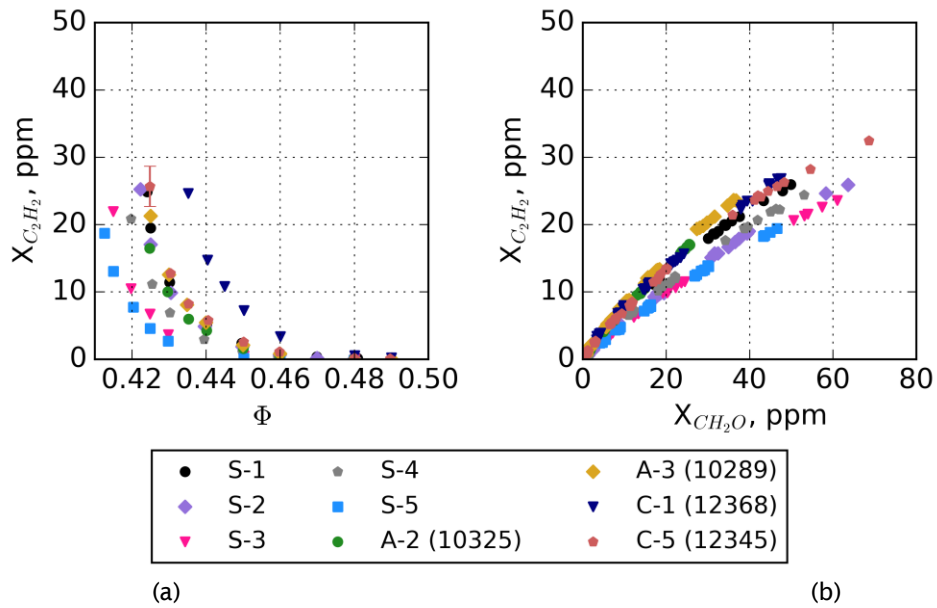


Figure 14. Acetylene (C_2H_2) as a function of equivalence ratio (Φ) sampled from the FTIR. (a) Points represent the average of the data at each equivalence ratio, while the error bars represent the maximum standard deviation in the reported set. (b) Points represent the all the sampled data as a function of formaldehyde.

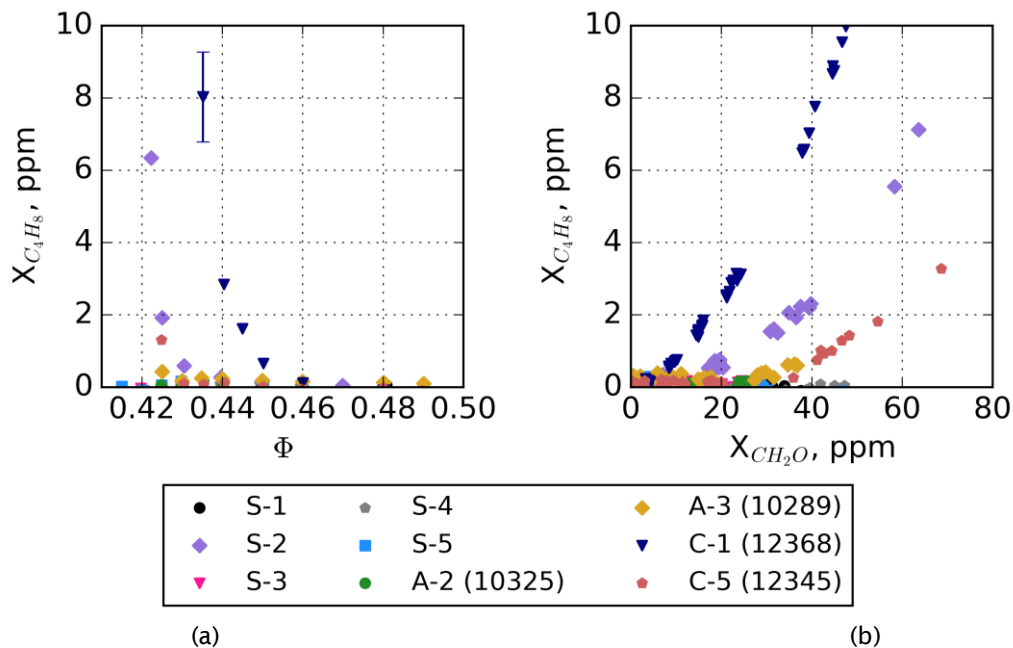


Figure 15. Isobutene (C_4H_8) as a function of equivalence ratio (Φ) sampled from the FTIR. (a) Points represent the average of the data at each equivalence ratio, while the error bars represent the maximum standard deviation in the reported set. (b) Points represent the all the sampled data as a function of formaldehyde.

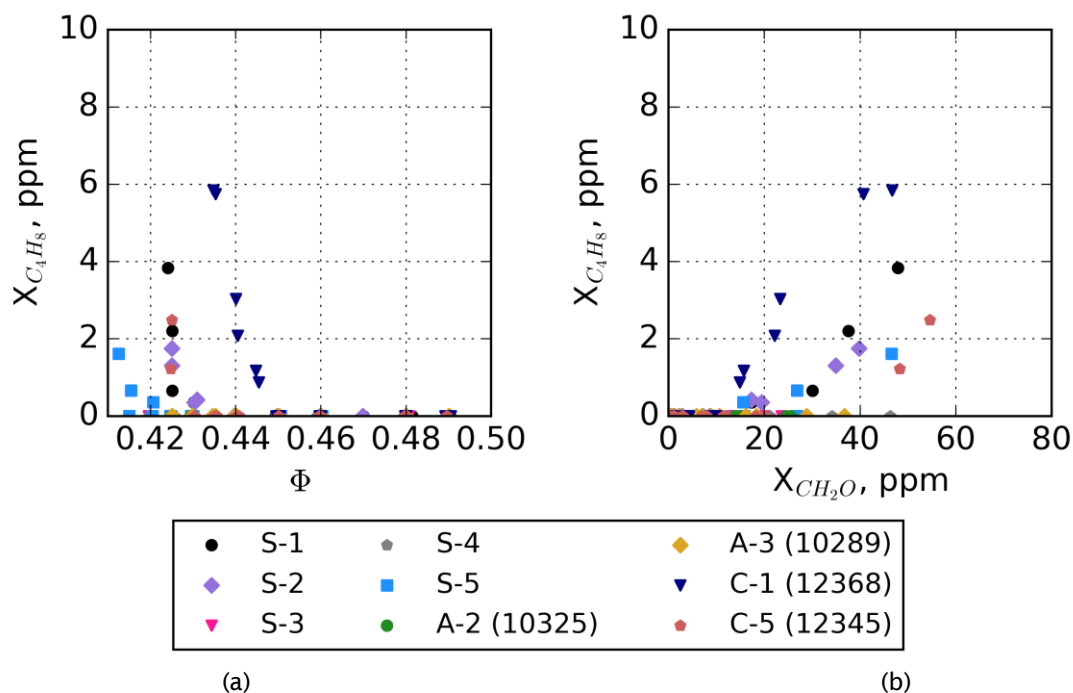


Figure 16. Isobutene (C_4H_8) as a function of equivalence ratio (Φ) from the charcoal tube methodology. (a) Points and samples taken during testing at the end of each condition as a function of equivalence ratio. (b) Points and samples taken during testing at the end of each condition as a function of formaldehyde.

Additional efforts were made with the Well-Stirred Reactor to refine the LBO measurements. The previous procedure towards LBO provided the ability to obtain steady state emissions measurements within the WSR approaching LBO. A new technique was integrated into the data acquisition system to decrease the fuel flow rate automatically, keeping the air flow rate constant, as in previous experiments. This procedure allows for multiple LBO measurements to be made within a single test run per fuel. The fuels tested with this new approach were selected to stress-test the DCN hypothesis.

Table 4: Fuels tested in the WSR using the new LBO procedure (*S-1 from Won, et. al. 2017).

Name	DCN	Nomenclature
Dodecane (n-C12)	74	C_{12}
Surrogate Fuel 1*	50.4	S-1
NJFCP A-2	48.3	A-2
NJFCP C-4	28	C-4
75.5% 135 TMB, 24.5% n-C12	19.08	J-1
NJFCP C-1	17.1	C-1

Dodecane was selected on the upper bound of the DCN that was tested, where C-1 was the lower bound to the DCN. Additional fuels tested as part of the NJFCP program include A-2 and C-4. A surrogate fuel to emulate the characteristics of



NJFCP A-2 and given combustion property targets was additionally selected, named S-1 (Won, et. al., 2017). An additional fuel, J-1, comprised of 1,3,5 trimethylbenzene (135 TMB) and dodecane, was added to investigate the effect of radical index at a lower DCN to investigate radical pooling effects towards extinction, as previously discussed. Number of ramp rates performed with LBO testing was 13 for the fuels except Dodecane (5 samples for Dodecane). A lean equivalence ratio usually around 0.45, above the extinction limit, was established before decreasing the equivalence ratio 0.001 (~0.05 mL/min using the Isco pumps for the fuel) every 4 seconds. This ramp rate was chosen to reduce wall effects on LBO that are around the outer surface of the reactor and to establish a steady decrease in reactor temperature as minimizing transient effects are optimal. LBO is reached when there exists a significant temperature drop from the previous value. The tradeoff with this approach is that emissions sampling was reduced to only the FTIR online sampling, as the duration of capturing the emissions using the gas bags and charcoal tube measurements takes longer than the ramp rate utilized in the experiment. Data acquisition from the 5Hz online MKS 2030 HS gas analyzer was averaged and matched to the time histories of the other experimental data captured (0.5 Hz). The gas analyzer was the same as previously used in the other experiments.

LBO and emissions towards LBO are presented in the figures below. Fig. 17 shows the linear correlation between the LBO and DCN of the corresponding fuels. Error bars on the figure represent the standard deviation of the LBO J-1 and C-1 both yield similar LBO values, although the chemical compositions are vastly different, and their radical index is different. High percentages of aromatics as seen in the J-1 fuel also decreases the resistance to LBO, whereas the C-1 fuel is comprised of the iso-paraffinic compounds. S-1 and A-2 have been observed to have similar LBO values, as expected. Dodecane is also seen to have the lowest LBO value and having the highest DCN value. Emissions profiles for ethylene and isobutene are plotted as functions of equivalence ratio and formaldehyde. An exponential increase in emissions is seen similarly to the other experiment performed in the WSR. As leaner conditions are approached towards LBO, there is a reduction in combustion efficiency, where incomplete reactions are occurring, not converting the fuel to the CO₂ and H₂O and is seen in the figures. S-1 emissions trends yield similarity to A-2, further establishing similarity between a surrogate fuel mixture comprised of 3 compounds to a jet-fuel comprised of multiple components. Emissions as a function of formaldehyde has been presented as formaldehyde is a marker for the incomplete combustion and for other pollutant emissions to be generated. Non-linearity is presented towards higher amounts of formaldehyde production and shows the instability towards the extinction process.

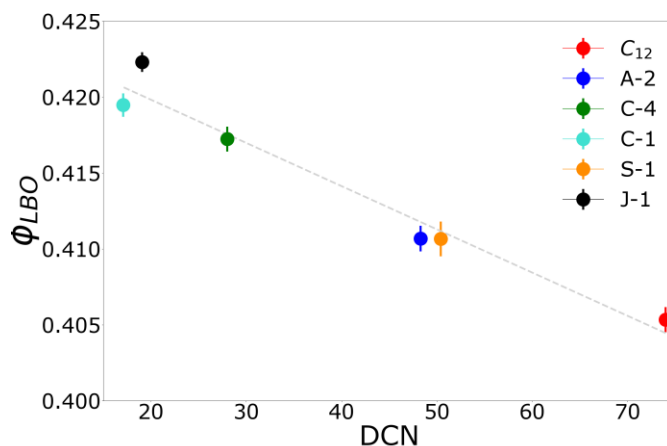


Figure 17: LBO as a function of DCN. The R² value based off a linear fit is 0.9581 ($-2.8466E-04 * DCN + 0.42552 = \phi_{LBO}$).

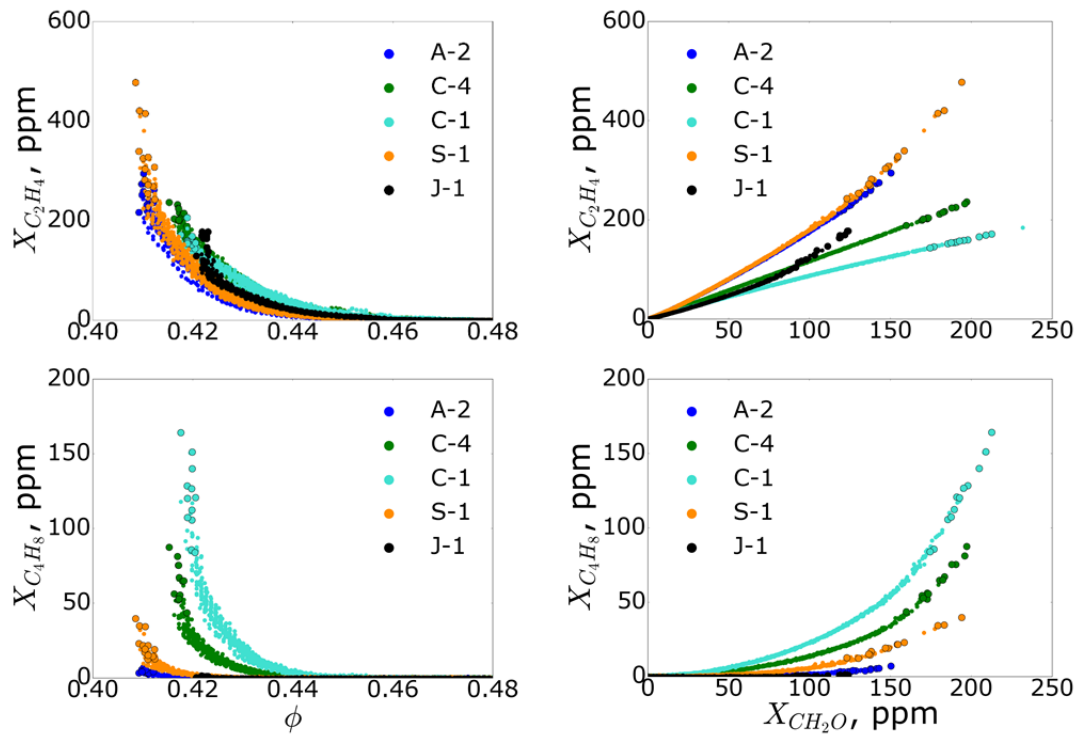


Figure 18: Emissions v. ϕ_{LBO} for the WSR. (R side) Emissions v. CH_2O for the WSR. A-2 and S-1 data trends similarly with each other.

IV. Conclusions

A WSR operating under fuel-lean conditions was utilized to measure performance and gaseous emissions characteristics of conventional and alternative aviation fuels. LBO was also explored under the same loading condition to determine the difference in LBO with different fuels. The experiment showed:

1. Recovery of carbon captured is favorable from the FTIR and can provide encouraging results with the current species captured.
2. The C-1 test fuel is least resistant to LBO as the conditions for which it occurs happens at a higher equivalence ratio and at a higher reactor temperature than the other tested fuels.
3. LBO shows a strong correlation with derived cetane number, which describes a need for investigating fuel dependency on combustor design.
4. As conditions approach LBO, intermediate species are produced that have a correlation between formaldehyde productions. These conditions towards LBO signify decreased combustion efficiency as more intermediate species are seen.
5. S-1 yielded similar performance characteristics in the WSR as A-2.

Continued analysis will enable investigation of chemical kinetic pathways specific to each fuel, which then establishes an understanding of the chemical effects in a lean, premixed, prevaporized environment, a relevant area of interest for future gas turbine combustor design. The WSR represents an ideal, premixed, pre-vaporized combustor. It is used to study fuel chemistry effects on emissions and LBO. Thus, we believe the knowledge gained from the fuel effects in our LBO and emissions studies have relevance to current and future combustion systems.



References

- AJF-IWG. 2016. "Federal Alternative Jet Fuels Research and Development Strategy." OSTP.
- Anneken, David, Richard Striebich, Matthew J. DeWitt, Christopher Klingshirn, and Edwin Corporan. 2014. "Development of Methodologies for Identification and Quantification of Hazardous Air Pollutants from Turbine Engine Emissions." *Journal of the Air & Waste Management Association* 65 (3): 336–46. doi:10.1080/10962247.2014.991855.
- Blunck, D, J Cain, Rc Striebich, Sz Vijlee, Sd Stouffer, and Wm Roquemore. 2012. "Fuel-Rich Combustion Products from a Well-Stirred Reactor Operated Using Traditional and Alternative Fuels." *Central States Combustion Meeting*, 1–8.
- Blunck, David L., Steven Zeppieri, Justin T. Gross, Scott Stouffer, and Meredith B. Colket. 2015. "Hydrocarbon Emissions from a WSR Near Lean Blow-Off." In *53rd AIAA Aerospace Sciences Meeting*, 1–12. Kissimmee, FL: American Institute of Aeronautics and Astronautics. doi:10.2514/6.2015-0415.
- Blust, J., D. Ballal, and G. Sturgess. 1997. "Emissions Characteristics of Liquid Hydrocarbons in a Well Stirred Reactor." In *33rd AIAA/ASME/SAE/ASEE Joint Propulsion Conference & Exhibit*, 1–18. Seattle, WA: AIAA. doi:10.2514/6.1997-2710.
- Blust, J. W., D R Ballal, and G J Sturgess. 1999. "Fuel Effects on Lean Blowout and Emissions from a Well-Stirred Reactor." *Journal of Propulsion and Power* 15 (2): 216–23. doi:10.2514/2.5444.
- Briones, AM, B Sekar, J Zelina, R Pawlik, and SD Stouffer. 2008. "Numerical Modeling of Combustion Performance for a Well-Stirred Reactor for Aviation Hydrocarbon Fuels (AIAA-2008-4565)." In *44th AIAA/ASME/SAE/ASEE Joint Propulsion Conference & Exhibit*, 1–19. Hartford, CT: AIAA. doi:doi:10.2514/6.2008-4565.
- Colket, Meredith B., Joshua S. Heyne, Mark Rumizen, James T. Edwards, Mohan Gupta, William M. Roquemore, Jeffrey P. Moder, Julian M. Tishkoff, and Chiping Li. 2016. "An Overview of the National Jet Fuels Combustion Program." In *AIAA SciTech*. AIAA SciTech. San Diego, CA: American Institute of Aeronautics and Astronautics. doi:doi:10.2514/6.2016-0177.
- FAA. 2012. "U.S. Aviation Greenhouse Gas Emissions Reduction Plan," no. June: 1–16.
- Karalus, Megan. 2013. "An Investigation of Lean Blowout of Gaseous Fuel Alternatives to Natural Gas." University of Washington.
- Manzello, Samuel L., David B. Lenhert, Ahmet Yozgatligil, Michael T. Donovan, George W. Mulholland, Michael R. Zachariah, and Wing Tsang. 2007. "Soot Particle Size Distributions in a Well-Stirred Reactor/plug Flow Reactor." *Proceedings of the Combustion Institute* 31 (1): 675–83. doi:10.1016/j.proci.2006.07.013.
- McAllister, Sara, Jyh-Yuan Chen, and A. Carlos Fernandez-Pello. 2011. *Fundamentals of Combustion Processes*. Mechanical Engineering Series. New York, NY: Springer New York. doi:10.1007/978-1-4419-7943-8.
- Mensch, Amy. 2009. "A Study on the Sooting Tendency of Jet Fuel Surrogates Using the Threshold Soot Index." M.S. Thesis. The Pennsylvania State University.
- Nenniger, J.E., A. Kridiotis, J. Chomiak, J.P. Longwell, and A.F. Sarofim. 1984. "Characterization of a Toroidal Well Stirred Reactor." *Twentieth Symposium (International) on Combustion*. The Combustion Institute, 473–79.
- Stouffer, S, R C Striebich, C W Frayne, and J Zelina. 2002. "Combustion Particulates Mitigation Investigation Using a Well-Stirred Reactor." In *38th AIAA/ASME/SAE/ASEE Joint Propulsion Conference and Exhibit*, 1–11. Indianapolis, IN: American Institute of Aeronautics and Astronautics. doi:10.2514/6.2002-3723.
- Stouffer, Scott D, Dilip R Ballal, Joseph Zelina, Dale T Shouse, Robert D Hancock, and Hukam C Mongia. 2005. "Development and Combustion Performance of High Pressure WSR and TAPS Combustor." In *43rd AIAA Aerospace Sciences Meeting and Exhibit*, 1–9. Reno, NV: American Institute of Aeronautics and Astronautics. doi:10.2514/6.2005-1416.
- Stouffer, Scott, Robert Pawlik, Garth Justinger, Joshua Heyne, Joseph Zelina, and Dilip Ballal. 2007. "Combustion Performance and Emissions Characteristics for a Well Stirred Reactor for Low Volatility Hydrocarbon Fuels." In *43rd AIAA/ASME/SAE/ASEE Joint Propulsion Conference and Exhibit*, 1–12. Cincinnati, OH: American Institute of Aeronautics and Astronautics. doi:10.2514/6.2007-5663.
- Vijlee, Shazib Z. 2014. "Effects of Fuel Composition on Combustion Stability and NOX Emissions for Traditional and Alternative Jet Fuels." University of Washington.



- Won, Sang Hee, Stephen Dooley, Frederick L Dryer, and Yiguang Ju. n.d. "Radical Index on Extinction Limits of Diffusion Flames for Large Hydrocarbon Fuels." doi:10.2514/6.2011-318.
- Won, Sang Hee, Peter S Veloo, Jeffrey Santner, Yiguang Ju, and Frederick L Dryer. n.d. "Comparative Evaluation of Global Combustion Properties of Alternative Jet Fuels." doi:10.2514/6.2013-156.
- Won, Sang Hee, Peter S Veloo, Jeffrey Santner, Yiguang Ju, Frederick L Dryer, and Stephen Dooley. n.d. "Characterization of Global Combustion Properties with Simple Fuel Property Measurements for Alternative Jet Fuels." doi:10.2514/6.2014-3469.
- Won, S. H., Haas, F. M., Dooley, S., Edwards, T., and Dryer, F. L., "Reconstruction of chemical structure of real fuel by surrogate formulation based upon combustion property targets," Combustion and Flame, vol. 183, Sep. 2017, pp. 39-49.
- Wordland, Justin. 2015. "What to Know About the Historic 'Paris Agreement' on Climate Change."
- Yanowitz, J, Ecoengineering M A Ratcliff, R L McCormick, J D Taylor, and M J Murphy. 2004. "Compendium of Experimental Cetane Numbers."
- Zelina, Joseph. 1995. "Combustion Studies in a Well-Stirred Reactor." University of Dayton.

Milestone(s)

Measured LBO, a Figure of Merit in the NJFCP, for 4 fuels. Results are consistent with the more complicated Area 6 Referee Rig.

Major Accomplishments

Reporting LBO equivalence ratios for four NJFCP fuels.

Publications

Peer-reviewed Publications:

None. (One publication is in preparation.)

Conference Proceedings:

Stachler, Robert D., Joshua S. Heyne, Scott D. Stouffer, Joseph D. Miller, and William M. Roquemore. 2017. "Investigation of Combustion Emissions from Conventional and Alternative Aviation Fuels in a Well-Stirred Reactor." In 55th AIAA Aerospace Sciences Meeting. Grapevine, TX: American Institute of Aeronautics and Astronautics.

Outreach Efforts

Conference presentations:

- Stachler, Robert D., Joshua S. Heyne, Scott D. Stouffer, Joseph D. Miller, and William M. Roquemore. 2017. "Investigation of Combustion Emissions from Conventional and Alternative Aviation Fuels in a Well-Stirred Reactor." 55th AIAA Aerospace Sciences Meeting. Grapevine, TX: American Institute of Aeronautics and Astronautics.
- Stachler, Robert D., Joshua S. Heyne, Scott D. Stouffer, Joseph D. Miller, and William M. Roquemore. 2016. "Investigation of Combustion Emissions from Conventional and Alternative Aviation Fuels in a Well-Stirred Reactor." 12th Annual Dayton Engineering Sciences Symposium. Dayton, OH: ASME.

Awards

Joshua Heyne – SOCHE Faculty Excellence Award
Robert Stachler – ASME Outstanding Young Engineer

Student Involvement

Robert Stachler, Ph.D. student, leads this effort.



Plans for Next Period

It is planned to continue with additional LBO tests for the remaining NJFCP fuels (i.e. the remaining category A and C fuels as well as the fuel blends and surrogate blends).

Task #3: Cross-Experiment Analysis

University of Dayton

Objective(s)

The objective of this task is to link low cost fundamental experiments to larger cost more complicated experiments internal to the NJFCP.

Research Approach

Our current approach is linking experiments within the NJFCP via Random Forest Regression Analysis. This regression technique is advantageous for several reasons: 1) it can handle diverse sets of data with both qualitative and quantitative information, 2) it is a relatively unbiased regression technique, 3) the regression is a white-box approach, and 4) the regression can output the relative importance of various fuel and experimental features. More details regarding Random Forest Regression Analysis can be found elsewhere e.g., (Hastie, Tibshirani, and Friedman 2009).

Initial Results

We have been able to compile the data from Area 3 and 6 as well as the data from the WSR studies on LBO. Lean Blowout (LBO) is typically defined as the lower limit equivalence ratio that a geometry at a given condition can sustain a flame. This limit is of particular interest in relation to alternative fuel certification, as it represents an engine operability limit. If an aircraft that is designed to operate with conventional Jet-A fails to hold a flame under similar conditions with an alternative

Table 5: Summary of LBO rigs with fuels tested reported. Additional data, beyond that of LBO ϕ s, was taken for the rigs and fuels below. These additional data and results can be gleaned from companion papers (Chtev et al. 2017; S. D. Stouffer et al. 2017; Stachler et al. 2017).

Rig Name	Geometry type (injector/swirler)	T _{air}	T _{fuel}	P	Institution
PA-GT	Pressure atomizer/ Pratt & Whitney Swirler	550, 450, 300 K	445-460 K	3.4 atm	Georgia Tech
AB-GT	Air blast atomizer/ Pratt & Whitney Swirler	450 K	445-460 K	3.4 atm	Georgia Tech
PA-HW	Pressure atomizer/ toroidal	324, 525, 557, 562, 394 K	288 K	1, 1.3, 1.4, 3.3, 5.7, 2 atm	Honeywell
PA-RR	Pressure atomizer/ High-Swirl (P03)	400 K	320 K	2 atm	AFRL/UDRI
PV-WSR	Prevaporized/ toroidal	450 K	450 K	1 atm	AFRL/UDRI
LDI-NASA	Lean Direct Injection	575, 645, 730, 830 K		6.8, 10.9, 17 atm	NASA
PA-SH	Pressure atomizer/ swirler stabilized	280, 310, 340 K			Sheffield
PA-OSU	Pressure atomizer/ swirler stabilized	470 K		1 atm	Oregon State
PA-CAM	Pressure in bluff-body/swirler stabilized	340 K	300 K	1 atm	Cambridge
UTRC		555, 494 K		8.64, 5.6 atm	UTRC
DLR	Pressure atomizer/ swirl stabilized	323, 373 K		1 atm	DLR Germany

*Future analysis of GT data is only for the 450 K testing.

fuel, thrust and/or power would be lost to important aircraft functions and potentially pose a safety risk. LBO is identified as a FOM for this reason, and the NJFCP has multiple works documenting LBO results (Chtev et al. 2017; S. D. Stouffer et al. 2017; Stachler et al. 2017; Khandelwal 2017; Sidney, Allison, and Mastorakos 2017; Allison, Sidney, and Mastorakos 2017; Podboy, Chang, and Moder 2017). Figure 1 shows the various inlet pressures and temperatures that have been tested for LBO while a brief description of the conditions and experimental configurations of the source data presented in this paper are outlined in Table 5.

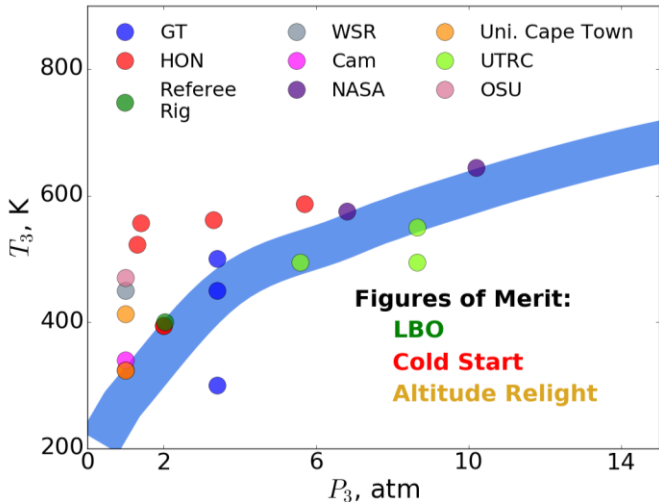


Figure 19. P₃-T₃ graphically displaying the rig conditions tested to measure the Figures of Merit (FOM), specifically for LBO tests for Georgia Tech (GT), Honeywell (HW), Referee Rig, Well-Stirred Reactor (WSR), Cambridge (Cam), NASA, University of Cape Town, UTRC, and Oregon State University (OSU).

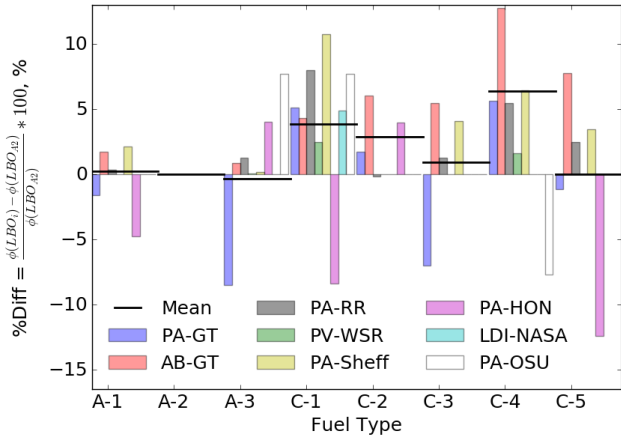


Figure 20: Nominal percent difference for Pressure Atomizer (PA), Lean Direct Injection (LDI), Air Blast (AB), and Pre-vaporized (PV) atomization/evaporation configurations using the Georgia Tech (GT), Referee Rig (RR), Well-Stirred Reactor (WSR), Sheffield (Sheff), Honeywell (HON), NASA, and Oregon State University (OSU) geometries versus A-2. The solid horizontal black line is the average for all tested fuels. C-1, C-2, and C-4 fuels are observed to be nominally different vs. A-2 for each experimental configuration. A-1, A-3, C-3, and C-5 are observed to blow off at equivalence ratios both leaner and richer than A-2 depending on the geometrical configuration. PA-GT bulk head temperatures are less than 550 K.

Year 3 of the program focused on the screening of NJFCP fuels in each experimental rig. Figure reports a box and whiskers plot illustrating the percent difference between A-2 and the various NJFCP fuels. The results are reported as a percent

difference from A-2 as the rigs display diverse ϕ s at LBO, i.e. typical (overall) LBO ϕ s for the Referee Rig are an order of magnitude more dilute than the Well-Stirred Reactor, since much of the air in an aero combustor is added subsequent to main combustion for liner cooling and dilution. The box and whisker plot shows significant scatter in the data for several fuels and rigs. The scatter in the data are not necessarily indicative of experimental shortcomings but are characteristic of the stochastic nature of limit phenomena and changing semi-controlled experimental conditions in the case of the Georgia Tech (GT) rig, as incremental bulk head temperatures/boundary conditions effect LBO. Finally, most fuels are found to have statistically similar LBO character, i.e. the whiskers overlap across fuels for a given geometrical configuration.

Significant systematic differences are observed across geometries as illustrated with Figure 6, which plots a geometry's root-mean-square (RMS) value across the fuels tested. The RMS value for a geometry is the variance the geometry produces for the variances in the NJFCP fuels. Geometries with relatively high RMS values are more sensitive to fuel variations, and conversely geometries with relatively small RMS values are less fuel sensitive.

To analyze the results collectively, a Random Forest regression analysis is performed on all the LBO data presented in this paper. For the analysis, the average percent difference for each fuel and configuration relative to the LBO ϕ of A-2 at similar conditions is evaluated relative to the chemical and physical properties of each fuel. It should be noted that some of these chemical and physical properties, when unavailable, are estimated via the methods described in Ref. (Bell et al. 2017). The regression results yielded results differing from previous reports and publications, e.g. Ref. (Lefebvre 1983),

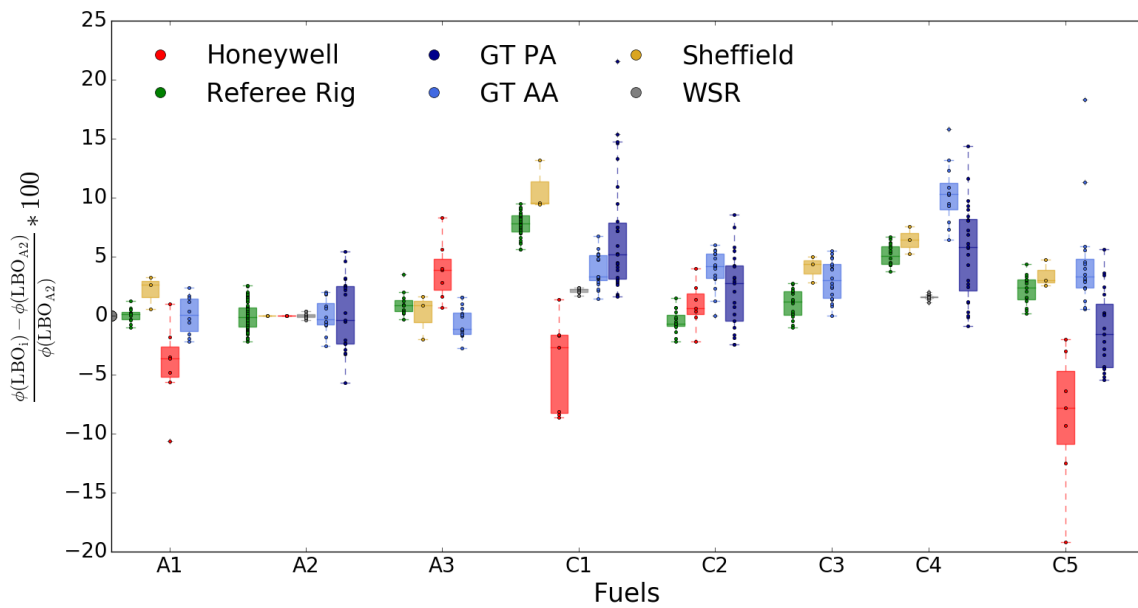


Figure 21: Box plot of percent difference LBO from A-2 for six NJFCP experimental configurations and eight fuels within the program. The circles represent individual observations, boxes represent the upper and lower 75 and 25 percentiles with the horizontal bar illustrating the median, the 'x' is the mean LBO value, the upper and lower bars are the first and fourth quartiles respectively, and data outside the quartiles are outliers. Experimental repeatability is greater than LBO differences between fuels. Fuel C-1 is observed to blow off at the richest equivalence ratios **relative to A-2**.

which implied stronger correlations to physical property effects versus the chemical property effect of DCN observed here. Beyond the reactivity effect of DCN on LBO, there is significant rig and atomizer geometry influence observed on the relative LBO of the fuels. The effect of fuel property effects and the aiding of the development of CFD models will be an area of continued investigation moving into Year 4 of the NJFCP. Finally, it should be noted that these regression techniques are in no way comprehensive in predicting LBO. The predictive capability of the current reported technique returns a R^2 value of approximately 0.85 for test data.

In Year 3 of the NJFCP, similar data analysis techniques were used to evaluate ignition results from different rigs throughout the program. Ignition at cold start and altitude relight conditions were stressed as both of these are also FOM

for the program. Figure 23 shows inlet temperature and pressure conditions tested for ignition while Table 3 outlines the various ignition test conditions and configurations used in the program to date.

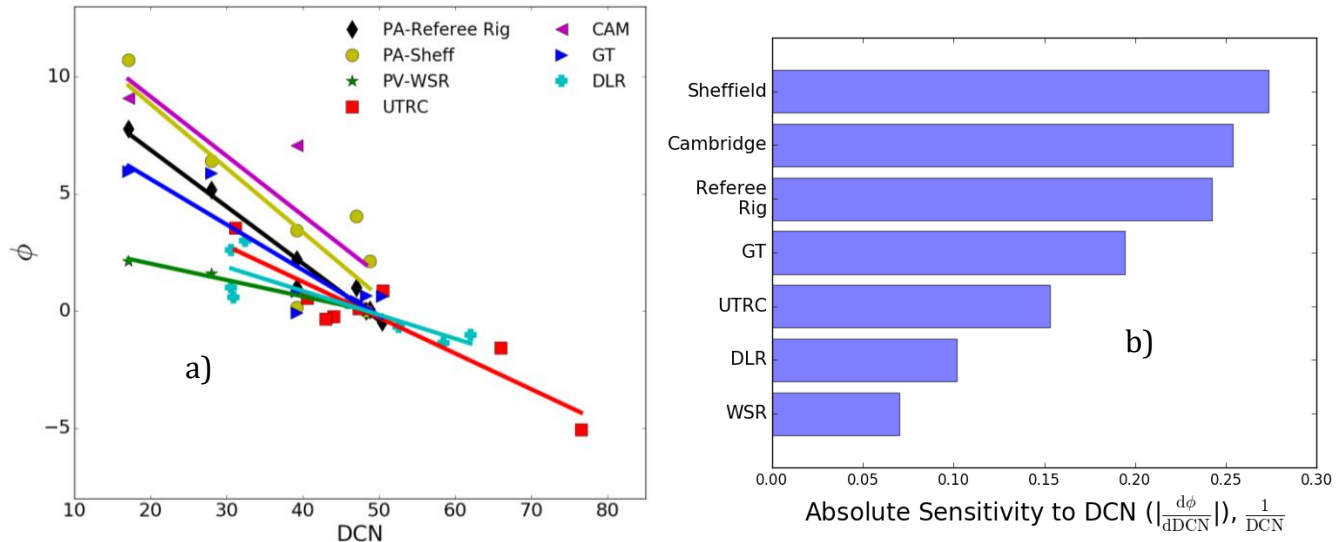


Figure 22: a) LBO Rig sensitivity to Derived Cetane Number (DCN) for seven NJFCP rigs. Whereas last year only three of the NJFCP rigs were shown to have a strong correlation with DCN for LBO, this year eight of the nine NJFCP rigs show this sensitivity (only seven shown here). The one rig that does not show this sensitivity is the Honeywell rig, the only rig that is not swirl stabilized. b) The bar graph on the left shows the Sheffield rig as being the most sensitive to DCN and the well-stirred reactor (WSR) as being the least sensitive. Note that ϕ represents percent difference LBO from A-2 for the category A and category C fuels.

Similar to LBO, Random Forest regressions were used as a way to determine feature importance from the chemical and physical properties, along with test conditions, when available in determining the ignition limit. Results have shown strong correlations to distillate properties and test conditions for the Honeywell rig, similar to what was found for LBO, while Georgia Tech prevaporized ignition tests have shown strong dependence primarily on test conditions. While the results for LBO over the last several years of the program were helpful in determining new properties that should be part of the alternative fuels certification process, ignition results so far have not presented any major new findings. As more ignition data is collected over the next year, more analysis will be done to gain better insight.

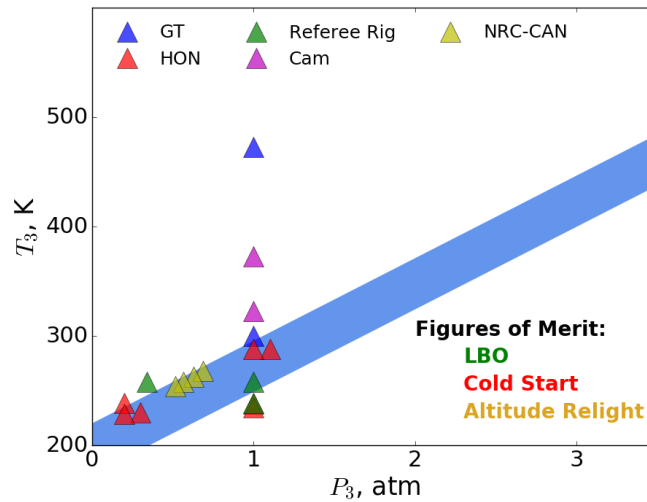


Figure 23: Ignition inlet pressure (P_3) and temperature (T_3) tested in Georgia Tech (GT), Honeywell (HON), Referee Rig, Cambridge (CAM), and NRC-Canada rigs. Ignition cold start and altitude relight were identified as two of the three FOM to be stressed in the program.

Table 6: Summary of Ignition rigs.

Rig Name	Rig Description	Ignition Source	T_{air}	T_{fuel}	P	Institution
NRC-CAN	Pressure atomizer in a small gas turbine engine (TRS-18)	Discharge	254 to 268 K	254 to 268 K	10-17 kft	NRC-CAN
Honeywell	Pressure Atomizer in APU	Discharge	230 to 317 K	236 and 288 K	0.2 to 1.1 atm	Honeywell
Cambridge	Partially Pre-vaporized flow Rig	Laser (YAG)	323 to 373 K		1 atm	Cambridge
GT - PV	Pre-vaporized fuel/air flow split from air coflow	Discharge	478 K	470 K	0.96 atm	Georgia Tech
AFRL/UDRI	Pressure atomizer, high swirl	Discharge	394 and 233 K	322 and 233 K	2 atm	AFRL/UDRI
GT - Spray	Pressure atomizer injected into air coflow	Discharge	293 to 478 K	470 K	0.96 atm	Georgia Tech



Milestone(s)

Presentation at the NJFCP Year-End Meeting. Contributing to the upcoming AIAA paper and presentation.

Major Accomplishments

We have shown strong evidence that LBO is most strongly predicted by the chemical property DCN across four experimental platforms in the NJFCP. This could potentially aid in developing blending rules for fuels to proceed through the ASTM approval process.

Publications

None.

Outreach Efforts

Oral presentations:

Carson, Jeremy, Joshua S. Heyne, Scott D. Stouffer, and Tyler Hendershott. 2016. "On the Relative Importance of Fuel Properties on LBO Behavior." 12th Annual Dayton Engineering Sciences Symposium. Dayton, OH: ASME.

Carson, Jeremy and Joshua S. Heyne. 2017. "Updates on the Relative Importance of Fuel Properties on LBO Behavior." 42nd Dayton-Cincinnati Aerospace Sciences Symposium. Dayton, OH: AIAA.

Peiffer, Erin, Joshua S. Heyne. 2017. "LBO, Ignition, and Spray Feature Importances from Year 3 of the National Jet Fuels Combustion Program." 13th Annual Dayton Engineering Sciences Symposium. Dayton, Ohio: ASME.

Awards

Jeremy Carson – Best presentation DESS 2016, Best presentation DCASS 2017.

Student Involvement

Jeremy Carson, Graduate Research Assistant, January 2015 – May 2017 (graduated), now at UDRI.
Erin Peiffer, Graduate Research Assistant, June 2017 - present.

Jennifer Colborn, Undergraduate Research Assistant, August 2016 – August 2017, now at UDRI.
Katherine Opacich, Undergraduate Research Assistant, November – 2017 – present.

Plans for Next Period

We plan to continue our current research technique incorporating greater depth into our results and incorporating additional data (i.e. spray) into our work.

Task #4: Common Format Routine Software Development

Alejandro Briones
Bob Olding
Mike Hanchak
Joshua Heyne

Objective(s)

We aim to develop a software package in which the OEMs can utilize the state of the art models being developed by the other NJFCP modeling teams.

Research Approach

This work is motivated for the imperative necessity of expediting combustor rig evaluation process for ASTM D4054 through improved combustion modeling capabilities. This fuel certification entails three main figures of merit, viz., lean blowout, ignition, and cold relight. Current fuel certification requires expensive and time-consuming experimental testing in gas turbine engines. State-of-the-art combustion models that could expedite this process are not readily available for original engine manufacturers (OEMs). The main objective of this work is to bridge the gap between state-of-the-art academic combustion models and industrial software. The second aspect of this project is to speed up the academic codes

for reaching industrial grade software category. The third aspect of this project involves verification and validation of this common format routine (CFR) software.

Modeling and simulation of complex fuels in gas turbine combustors is not trivial. Gas turbine combustors are intricate devices with characteristic length scales varying from the sub-millimeter laminar flamelet thickness to the large centimeter-size dilution holes. Therefore, the mesh resolution for gas turbine combustors is in the order of millions to even hundreds of million cells. The time scales associated with combustion and turbulence in the combustor vary from microseconds for the Kolmogorov turbulent length scales and species reaction rates to milliseconds associated with the flow through-time of the combustor. The time steps and mesh requirements for modeling and simulating a combustor are nearly prohibited. In order to mitigate some of the challenges associated with modeling and simulation of gas turbine combustors, the lower-dimensional manifold combustion (LDMC) models decouple the chemistry and chemistry-turbulence interaction from the complex turbulence computational fluid dynamics (CFD) calculations. The chemistry is computed *a priori* from one-dimensional stagnation flow equations and/or equilibrium calculation. The chemistry-turbulence interaction is computed by presuming probability density functions (PDFs). Transport equations for the moments of the mixture fraction (Z) and progress variable (C) are solved in the physical space. Then, these values are used to interpolate and to extract the thermo-chemical and transport information of the pre-tabulated table.

Commercial software such as Fluent [1,2] and Star-CCM+ already have built-in LDMC models. However, there are always limitations in terms of implementation. For instance, Fluent [1,2] pre-tabulates the table in a mixture fraction space directly. Hence, it does not solve for the one-dimensional equations. On the other hand, the CFR software presented in this paper uses a modified Cantera 2.3 [1] package. The CFR pre-tabulates chemical-turbulence interaction in the one-dimensional physical space. This allows the user to vary the transport coefficient formulation and investigated such effects on numerical predictions. Another difference between Fluent [1,2] and the CFR is that the latter can compute the three branches of the combustion phenomenon. Moreover, the CFR is more flexible because molecular properties are directly interpolated from the table. On the contrary, Fluent [1,2] does not offer this capability. Other commercial software package such as Chemkin [1] offers flamelet calculations that include the three branches of combustion. This software is very robust, but does not offer the turbulence-chemistry convolution capability needed for computing turbulent flames. To the best of our knowledge there is no standalone software that offers the capability of performing turbulence-chemistry convolution of a flamelet library. In addition, the CFR software is designed in a manner that more modules and capability can be easily annexed providing more flexibility to the user.

The purpose of this paper are to document the development of the CFR as well as to prove that such software has been verified and validated. Subsequently, the software is introduced. Important definitions are formulations are illustrated and discussed. Then, the verification and validation tests are presented.

Common Format Routine (Cfr) Software

In short, the CFR software can be sub-divided into two components, viz., the pretabulator and the flamelet-based software, which is illustrated in Appendix Figure 1. The pretabulator is capable of tabulating thermo-chemical and transport data for laminar and turbulent flames. The pretabulator is based on a modified version of Cantera 2.3 [3]. Cantera is written in C++ and Python wrappers/codes were developed in order to include new capabilities in Cantera. This Python codes also interact with a C# GUI. This can currently tabulate flamelet prolongation of the intrinsic low-dimensional manifold (FPI) and flamelet progress variable (FPV). The flamelet-based software can attach the pretabulated turbulence-chemistry interaction table to a CFD code. In this case the flamelet-based software was attached to Fluent [1,2]. The flamelet-based software machinery can perform bilinear, trilinear and tetralinear interpolation of this thermochemical table. This software is written in C and its GUI is written using C#. Now detailed description of the software is provided next.

A. Mixture Fraction Definition

Mixture fraction is a conserved scalar. This means that mixture fraction cannot be created or destroyed. Because atomic elements and enthalpy cannot be created or destroyed, mixture fractions is typically defined in this context. Here the mixture fraction is defined in terms of atomic elements and any combination of atomic elements is valid. However, the atomic composition needs to be chosen so that mixture fraction varies between zero and unity.

$$Z = \sum_{i=1}^{N_{atomic\ selection}} \sum_{n=1}^{N_{species}} \frac{MW_i}{MW_n} Y_n \quad (1)$$

The user selection of the mixture fraction definition is given by Appendix Figure A 2.

B. Progress Variable Definition

The progress variable provides quantitative information of the combustion efficiency. The latter is equal to zero when the flame blows out and combustion efficiency is zero. The maximum value of the progress variable is a real number less than unity. The progress variable is defined in terms of species mass fractions. The equation below indicates that the mixture fraction is the summation of species mass fractions. Typically in the literature CO and CO₂ are selected to indicate the level of completeness of the combustion process. In addition, CO, CO₂, H₂ and H₂O are also chosen species to indicate the combustion efficiency (or completeness of the combustion process).

$$C = \sum_{n=1}^{N_{species\ selected}} Y_n \quad (2)$$

The user selection of the mixture fraction definition is given by Appendix Figure A 3.

C. Progress Parameter Definition

For premixed and diffusion flamelets, the progress variable defined by Eq. (2) varies in the spatial direction. For a premixed flamelet C increases monotonically from the unburned reactants from zero to a maximum value downstream the flame front. For diffusion flamelets the behavior is non-monotonic and the maximum value of C occurs near stoichiometry and then its value decreases to zero towards the reactant inlets. Therefore, the progress variable definition is a function of mixture fraction, i.e. $C = C(Z)$. Thereby, the progress parameter Λ is defined as a bijective, unique identifier that can be used to sort each flamelet. This definition is given below.

$$\Lambda = f(C, Z) \quad (3)$$

This definition is particularly useful for modeling diffusion flamelets and has been implemented in the current software. In the CFR this conversion can be enable or disable.

D. Convoluted Thermochemical and Transport Variables

Once state relationships have been computed between thermochemical and transport properties and the lower dimensional manifold variables (i.e., Z and Λ) these quantities need to be convoluted for the turbulence-chemistry interaction using the equation below. The probability density functions (PDF) in this equation reads as "the probability density function of Z as a function of \tilde{Z} and $\tilde{Z}^{\prime 2}$." Then, all thermochemical and transport properties (ϕ) such as density (ρ), molecular weight (MW), temperature (T), specific heat capacity (c_p), dynamic viscosity (μ), thermal conductivity (k), species mass fractions (Y_i) and species reaction rates ($\dot{\omega}_i$) are a function of the transported lower-dimensional manifold variables (\tilde{Z} , $\tilde{Z}^{\prime 2}$, $\tilde{\Lambda}$ and $\tilde{\Lambda}^{\prime 2}$).

$$\tilde{\phi}(\tilde{Z}, \tilde{Z}^{\prime 2}, \tilde{\Lambda}, \tilde{\Lambda}^{\prime 2}) = \int_0^1 \int_0^1 \phi(Z, \frac{\Lambda}{\Lambda_{max}}) PDF(Z; \tilde{Z}, \tilde{Z}^{\prime 2}) PDF(\frac{\Lambda}{\Lambda_{max}}; \tilde{\Lambda}, \tilde{\Lambda}^{\prime 2}) dZ d\Lambda \quad (4)$$

Importantly to note is that the above equation, the progress parameter requires normalization before integration.

E. Lower Dimensional Manifold Transported Variables For Laminar Flows

Equations (5) and (6) are mixture fraction (Z) and progress variable (C) transported equations. When solving for laminar flows convolutions such as that represented by (4) are not necessary. Both equations here contain a transient, a convective and a diffusive term. However, the progress variable in addition contains a source term Ω_C .



$$\frac{\partial(\rho Z)}{\partial t} + \frac{\partial(\rho Z u_j)}{\partial x_j} = \frac{\partial}{\partial x_j} \left(\frac{\lambda}{c_p} \frac{\partial Z}{\partial x_j} \right) \quad (5)$$

$$\frac{\partial(\rho C)}{\partial t} + \frac{\partial(\rho C u_j)}{\partial x_j} = \frac{\partial}{\partial x_j} \left(\frac{\lambda}{c_p} \frac{\partial C}{\partial x_j} \right) + \dot{\Omega}_C \quad (6)$$

The source term ($\dot{\Omega}_C$) is computed as follows,

$$\dot{\Omega}_C = \sum_{i=1}^{N_{\text{species selected}}} \dot{\Omega}_i \quad (7)$$

Hence, the definition of Eq. (7) has to be consistent with the definition of Eq. (2). Then, all thermochemical and transport properties such as density (ρ), molecular weight (MW), temperature (T), specific heat capacity (c_p), dynamic viscosity (μ), thermal conductivity (k), species mass fractions (Y_i) and species reaction rates ($\dot{\omega}_i$) are a function of the transported lower-dimensional manifold variables. The progress parameter can be obtained via Eq. (3).

F. Lower Dimensional Manifold Transported Variables For Turbulent Flows

The transport equations for the lower-dimensional manifold variables (i.e., mixture fraction (\tilde{Z}), mixture fraction variance ($\tilde{Z}^{\prime 2}$), and progress variable (\tilde{C}) are illustrated by equations (8)-(10) in tensor notation (and in conservative form) in the context of either the unsteady Reynolds-Averaged Navier Stokes (URANS) or Large-eddy simulation (LES) turbulence model formulations. For the former formulation the dependent variable represents the Favre-weighted time-averaged variable whereas for the latter the dependent variable represents the Favre-weighted filtered variable. Equations (8) through (10), respectively, correspond to the mixture fraction (\tilde{Z}), mixture fraction variance ($\tilde{Z}^{\prime 2}$), and progress variable (\tilde{C}).

1. Transport Equations

The transported equations of the lower-dimensional manifold variables contain at least three terms, viz., transient, convection and diffusion. The mixture fraction variance in addition contains a destruction and production of $\tilde{Z}^{\prime 2}$ represented by the last two terms of Eq. (9), respectively. The progress variable transport equation also contains a source term represented by the last term of Eq. (10).

$$\frac{\partial(\bar{\rho}\tilde{Z})}{\partial t} + \frac{\partial(\bar{\rho}\tilde{Z}u_j)}{\partial x_j} = \frac{\partial}{\partial x_j} \left(\left(\frac{\lambda}{c_p} + D_t \right) \frac{\partial \tilde{Z}}{\partial x_j} \right) \quad (8)$$

$$\begin{aligned} \frac{\partial(\bar{\rho}\tilde{Z}^{\prime 2})}{\partial t} + \frac{\partial(\bar{\rho}\tilde{Z}^{\prime 2}u_j)}{\partial x_j} &= \frac{\partial}{\partial x_j} \left(\left(\frac{\lambda}{c_p} + D_t \right) \frac{\partial \tilde{Z}^{\prime 2}}{\partial x_j} \right) - \bar{\rho}\tilde{\chi}_Z \\ &+ 2\bar{\rho}D_t \left(\frac{\partial \tilde{Z}}{\partial x_j} \right)^2 \end{aligned} \quad (9)$$

$$\frac{\partial(\bar{\rho}\tilde{C})}{\partial t} + \frac{\partial(\bar{\rho}\tilde{C}u_j)}{\partial x_j} = \frac{\partial}{\partial x_j} \left(\left(\frac{\lambda}{c_p} + D_t \right) \frac{\partial \tilde{C}}{\partial x_j} \right) + \bar{\rho}\dot{\omega}_C \quad (10)$$

2. Closure Models

For RANS, SAS, DES and LES models the scalar dissipation rate associated with the progress variable (C) is as computed as follows [5].

$$\tilde{\chi}_C = \gamma_C \frac{\tilde{Z}^{\prime 2}}{\tilde{C}^2} \tilde{\chi}_Z \quad (11)$$

The closure models for the RANS-based lower-dimensional manifold transported variable equations are given by the following equations [5].

$$D_t = \frac{\mu_t}{Sc_t} \quad (12)$$

$$\tilde{\chi}_Z = 2.0 \frac{\epsilon}{k} \tilde{Z}^{\prime 2} \quad (13)$$

The turbulent Schmidt number (Sc_t) is a constant that is typically chosen to be equal to 0.9. The closure models for the LES-based lower-dimensional manifold transported variable equations are given by the following equations [5].



$$D_t = C_\phi \Delta^2 |S| \quad (14)$$

$$\tilde{\chi}_Z = 2.0 \frac{\mu_t}{Sc_t} \frac{1}{\Delta^2} \tilde{Z}^2 \quad (15)$$

The constant C_ϕ is typically chosen to be equal to 0.4.

G. Low-Dimensional Manifold Combustion Models

The flamelet prolongation of ILDM (FPI) and the flamelet/progress variable (FPV) model utilize the one-dimensional stagnation flow equations for computing freely-propagating premixed flames and counterflow diffusion flames, respectively. The freely-propagating premixed flamelets of the FPI model are computed in the physical space and each flamelet is converted to the progress variable space (C) using Eq. (2). In turn, each premixed flamelet correspond to a mixture fraction (Z), which is directly related to an equivalence ratio. On the other hand, FPV model invokes the calculation of multiple diffusion flames. Each flame is computed in the physical space as well. The physical space can be converted to a mixture fraction state relationship (Z) following Eq. (1). Each flamelet correspond to a progress parameter (Λ). Therefore, calculations of multiple premixed and diffusion flamelets lead to a tabulation of thermochemical and transport properties as a function of mixture fraction (Z) and progress variable (C).

1. Transport Equations

The one-dimensional stagnation flow equations are presented above from Eqs. (16)-(21). In ascending order these equations represent the continuity, radial momentum, pressure curvature or strain rate eigenvalue, energy, species and a one-point or two-point dummy differential equation. The equations on the left of the table represent the original equations in Cantera 2.3 [3] for which the pressure curvature is the eigenvalue. The equations on the right represent the optional equations in a modified Cantera 2.3 in which strain rate (a) replaces the pressure curvature as the eigenvalue. The species and temperature equations are not modified. However, an additional dummy Eq. () was added to the governing equations for when the flame control methods are activated.


Table 7. Original and modified Cantera governing equations.

Equation	Cantera	Modified Cantera	
Continuity	$\frac{\partial \rho u}{\partial z} + 2\rho V = 0, V = \frac{v}{r}$	$\frac{\partial \rho u}{\partial z} + a\rho V = 0, V = \frac{v}{v_e}$	(16)
Radial Momentum	$\rho u \frac{\partial v}{\partial z} + \rho V^2 = -\Xi + \frac{\partial}{\partial z} \left(\mu \frac{\partial v}{\partial z} \right)$	$\rho u \frac{\partial v}{\partial z} = \frac{\partial}{\partial z} \left(\mu \frac{\partial v}{\partial z} \right) + \Xi(\rho_F - \rho V^2)$	(17)
Pressure Curvature/Strain Rate	$\frac{d\Xi}{dz} = 0, \Xi = \frac{1}{r} \frac{dP}{dr}$	$\frac{d\Xi}{dz} = 0, \Xi = a$	(16)
Energy	$\rho u c_p \frac{\partial T}{\partial z} = \frac{\partial}{\partial z} \left(\lambda \frac{\partial T}{\partial z} \right) - \sum_k j_k c_{p,k} \frac{\partial T}{\partial z} - \sum_k h_k W_k \dot{\omega}_k$		(19 17)
Species	$\rho u \frac{\partial Y_k}{\partial z} = -\frac{\partial j_k}{\partial z} + W_k \dot{\omega}_k$		(20)
One- or Two-point Control	$\frac{du_o}{dz} = 0$		(21)

2. Flamelet Prolongation of ILDM (FPI)

The FPI model computes premixed flamelets for each mixture fraction (Z). When the calculations do not converge because either the flamelets have exceeded the flammability limits or because the maximum temperature of the flamelet is higher than that of equilibrium, equilibrium calculations replace the freely-propagating premixed flamelets. The transport equations for the freely-propagating flamelets are given by Eqs. (22) - (26). The boundary conditions associated with the freely-propagating flamelets are shown in Table 8.

Table 8. Premixed flame boundary conditions.

Equation	Fuel Inlet	Oxidizer Inlet	
Continuity	-----	$\rho u = (\rho u)_o$	(22)
Radial Momentum	$V = V_F$	$V = V_o$	(23)
Pressure Curvature/Strain Rate	$\rho u = (\rho u)_F$	-----	(24)
Energy	$T = T_F$	$T = T_o$	(25)
Species	$\rho u Y_k + \rho Y_k V_k = (\rho u Y_k)_F$	$\rho u Y_k + \rho Y_k V_k = (\rho u Y_k)_o$	(26)

3. Flamelet Progress/Variable

The FPV model computes diffusion flamelets for each progress parameter (Λ) along the S-curve. Multiple diffusion flamelets are necessary to build a table of thermochemical and transport properties. The first flamelet is computed at $\Lambda_{max}|Z$ and then the strain rate is increased by either increasing the inlet velocities, reducing the distance between the opposing jets, or by either the one-point or two point continuation. The computation of diffusion flamelets as a function of strain rates leads to the calculation of the S-curve containing two stable branches (strong and weak) and one unstable (middle) branch. Special continuations techniques are needed to compute the S-curve associated with the diffusion flamelets. This will be discussed in subsequent chapters. The boundary conditions associated with the counterflow flamelets are shown in Table 9.

Table 9. Nonpremixed flamelet boundary conditions.

Equation	Inlet B.C.	Internal B.C.	Outflow B.C.	
Continuity	-----	$T_{j=specified} = T_{fixed,specified}$	-----	(18)
Radial Momentum	$V = V_o$	-----	$\frac{dV}{dz} = 0$	(19)
Pressure Curvature/Strain Rate	$\Xi = 0$	-----	-----	(20)
Energy	$T = T_o$	-----	$\frac{dT}{dz} = 0$	(21)
Species	$\rho u Y_k + \rho Y_k V_k = (\rho u Y_k)_o$	-----	$\frac{dY_k}{dz} = 0$	(22)



H. Continuation Methods

Continuation techniques are now presented, viz., zero-order, scaling rules, arc-length, and one- and two-point continuation techniques are presented. The zero-order continuation technique is used for FPI, whereas hybrid continuation techniques of zero-order, scaling rules, some features of arc-length continuation, and one- and two-point continuation techniques are used for the FPV model. The arc-length continuation technique was, however, fully utilized for perfectly-stirred reactors (PSRs) in order to progressively attain the now-used continuation technique for the FPV model. The arc-length continuation for PSR is only available in Python scripts and not through the GUI.

1. Zero Order Continuation

Zero-order continuation techniques can be applied to any flamelets. This technique only supposes that the previous solution is the initial solution to the current solution. This can be represented as $x^* = x_0$, where x refer to a vector solution with M grids points times N equations. This continuation methods can be applied to both FPI and FPV methods. For the former this is the only method available for continuation. For the latter the number of zero-order continuation can be selected from the Flame Control tab as illustrated in Appendix Figure 4.

Figure A 4

2. Scaling Rules

The scaling rules are ideal for computing the upper branch of S-curve. The scale factor proposed by Fiala and Sattelmayer [2] are suitable for the FPV model. These scaling factors are $u \sim a^{-1/2}$, $V \sim a$, $\dot{m} \sim a^{1/2}$, and $\Lambda \sim a^2$. The strain factor, which is the ratio of two sequential flame strain rates, can be entered by the user as illustrated in Appendix Figure 4.

3. Arc-Length Continuation

The system of nonlinear ODEs is represented by $F(x) = 0$. The solution is given by the vector x . The results of these equations depend on the parameter λ . The extended solution is represented by $F(x(\lambda), \lambda) = 0$. The arc-length continuation [3] is a predictor-corrector continuation technique.

1. Predictor:

One such predictor is the forward Euler predictor given by:

$$x^* = x_0 + \frac{dx}{ds} ds \quad (16)$$

The gradient dx/dF can be either a tangent or a secant gradient. Here the former is used. The predicted solution x^* is the initial guess for computing the new flame. The solution vector x that lies on the path depends on the parameter λ and this, in turn, depends on arclength s .

2. Corrector:

The plane equation parameterized as a function of arclength, s , needs to correct the initial guess x^* .

$$N(x(\lambda(s)), \lambda(s)) \equiv \left\| \frac{\partial x}{\partial s} \right\|_2^2 + \left(\frac{\partial \lambda}{\partial s} \right)^2 - 1 = 0 \quad (17)$$

Now the augmented systems of equations is given by:

$$\begin{cases} F(x(\lambda(s)), \lambda(s)) \\ N(x(\lambda(s)), \lambda(s)) \end{cases} = \begin{cases} 0 \\ 0 \end{cases} \quad (18)$$



This new vector can also be written as $G(F(y), N(y)) = 0$. The augmented solution vector is given by $y = (x(\lambda(s)), \lambda(s))$. The Jacobian matrix for the augmented system is represented by the following equation.

$$J = \begin{bmatrix} \frac{\partial F}{\partial x} & \frac{\partial F}{\partial \lambda} \\ \frac{\partial N}{\partial x} & \frac{\partial N}{\partial \lambda} \end{bmatrix} \quad (19)$$

The partial derivative of the plane equations needs to be determined from the plane equation:

$$N(x(\lambda(s)), \lambda(s)) \equiv \left\| \frac{\partial x}{\partial s} \right\| dx + \frac{\partial \lambda}{\partial s} d\lambda - ds = 0 \quad (20)$$

$$\frac{\partial N}{\partial x} = \left| \frac{\partial x}{\partial s} \right|^T \quad (23)$$

$$\frac{\partial N}{\partial \lambda} = \frac{\partial \lambda}{\partial s} \quad (22)$$

After substituting the equations above into the Jacobian, the augmented Jacobian is now given by:

$$J = \begin{bmatrix} \frac{\partial F}{\partial x} & \frac{\partial F}{\partial \lambda} \\ \left| \frac{\partial x}{\partial s} \right|^T & \frac{\partial \lambda}{\partial s} \end{bmatrix} \quad (23)$$

The augmented Jacobian and the residual equations are used in a Newton-Raphson type solver. The previous k solution is used to compute the new solution k+1.

$$y_{k+1} = y_k - J^{-1}G \quad (24)$$

The Newton-Raphson solver proceeds in this way. It computes the new change in the solution vector, Δy_k . This change is added to the solution vector of the previous iteration. Note that k=0 the values of $y_0[0: N_{eqs} - 2]$ are equal to the values of x^* .

$$J\Delta y_k = -G \quad (25)$$

$$y_{k+1} = y_k + \Delta y_k \quad (26)$$

$$\text{if } \Delta y_k < \varepsilon \rightarrow y_n = y_{k+1} \quad (27)$$

3. Step-size Control:

The user specifies an initial step size ds that is very large at first and the simulation proceeds. Near the turning points (bifurcations) the step size needs to become smaller in order to resolve the curve and avoid divergence of the Newton solver. Once the solution has passed the turning point the step size ds needs to increase again towards the other turning point. This is accomplished using the following step size control method.

$$\delta = N_{opt}/i_{Newton} \quad (28)$$

$$\text{if } \delta < 0.5 \rightarrow \delta = 0.5 \quad (29)$$

$$\text{if } \delta > 2.0 \rightarrow \delta = 2.0 \quad (30)$$

$$ds = \delta \cdot ds \quad (31)$$

This step size control technique works by allowing the user to specify the optimum number of Newton iterations, N_{opt} . If the number of Newton iterations i_{Newton} is below or above the N_{opt} the step size will increase or decrease, respectively. The multiplication factor δ is bounded between 0.5 and 2.0 in order to



avoid very small step size or very large step sizes that would either get the simulation stagnant or diverging. The step size control can be accessed through the Flame Control tab as illustrated in Figure A 55.

Some verification calculations are shown in Figure 24 through Figure 26 with numerical results available in the literature. There is nearly perfect match between previously computed S-curve for perfectly-stirred reactors (PSRs) and those computed here. This demonstrates that homotopic calculations and step size control are appropriately programmed for later used in the FPV tabulation procedure.

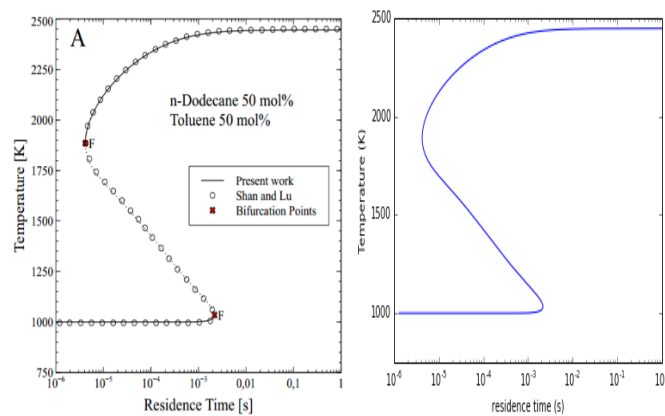
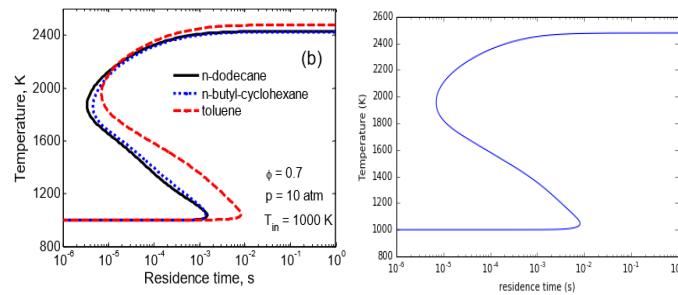


Figure 24. Comparison between Acampora and Marra [7] and in-house arc-length continuation for perfectly-stirred reactor (PSR). The inlet mass flow rate is the independent variable. Both temperature and residence time are output of the PSR. Reprinted from Computers and Chemical Engineering, 85, Acampora, L., Marra, F.S., A general study of counterflow diffusion flames at subcritical and supercritical conditions: Oxygen/hydrogen mixtures, with Permission from Elsevier



18.

Figure 25. Comparison between Shan and Lu [1] and in-house arc-length continuation for perfectly-stirred reactor (PSR) burning Toluene. The inlet mixture temperature is the independent variable.

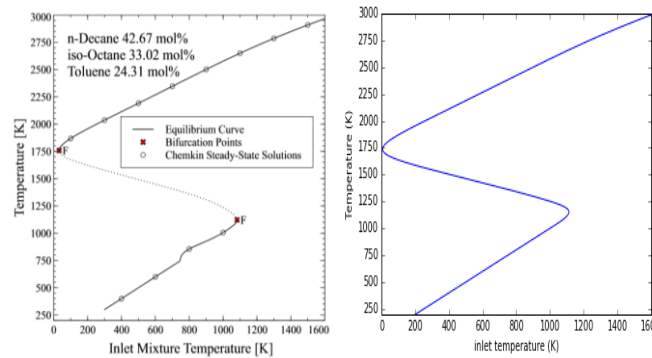


Figure 26. Comparison between Acampora and Marra [8] and in-house arc-length continuation for perfectly-stirred reactor (PSR). The inlet mixture temperature is the independent variable. Reprinted from Computers and Chemical Engineering, 85, Acampora, L., Marra, F.S., A general study of counterflow diffusion flames at subcritical and supercritical conditions: Oxygen/hydrogen mixtures, with Permission from Elsevier.

4. Flame Control Methods: One- and Two-Point

When the zero-order continuation and the scaling rules fail a flame control can be used to continue the bifurcation path of the S-curve. In the CFR this is automatically activated. The one- and two-point boundary conditions are based on the work of Nishioka et al. [8]. The boundary conditions for the pressure curvature or strain rate eigenvalue (Eq. (24)) is removed and replaced with an internal boundary condition (Eq. (24)) for the one-point continuation method. For the two-point continuation method the continuity equation boundary condition (Eq. (22)) is removed and a new internal boundary condition is added (Eq. (25)). For the one-point control method the oxidizer flux is specified as well as a fixed temperature on the fuel side. For the two-point control method neither the fuel nor the oxidizer flux are specified, but instead two fixed temperature location for the consecutive flamelet calculation at each side of the stagnation plane are prescribed.

Table 10. One- and two-point control boundary conditions.

Equation	Fuel Inlet	Internal B.C.	Internal B.C.	Oxid Inlet	
Pressure Curvature/ Strain Rate	-----	$T(j_{F,specified}) = T_{F,specified}$	-----	-----	(24)
Two-Point Control	-----	-----	$T(j_{O,specified}) = T_{O,specified}$		(25)

Figure 24 clearly shows that upper and middle branches can be successfully calculated with the CFR at low and high pressure conditions. Figure 5 illustrates the effect of transport model on the S-curve. There is a slight change on the S-curve for hydrogen-oxygen combustion. This is important because it suggests that the inexpensive unity Lewis number computation is sufficient for PSR without having to invoke more computationally-expensive calculations such as mixture-averaged diffusivity. Figure demonstrates that effect of varying the detailed chemistry. The same fuel-air composition is used with two different chemistry sets, but there is substantial change in the extinction strain rate.

Figure 27 shows the calculation of the S-curve for a more practical fuel used in gas turbine combustors.

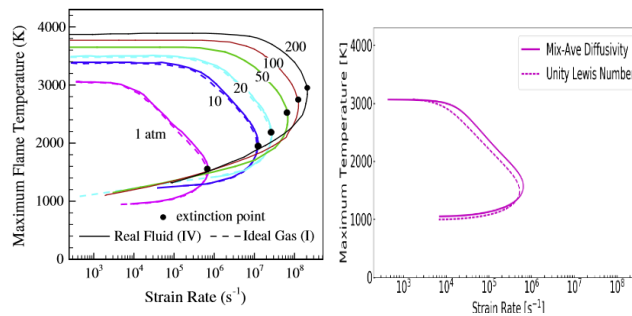


Figure 23. Comparison between mixture-averaged diffusivity and unity Lewis number. The mechanism used here is that of Burke et al. [13] Reprinted from *Combustion and Flame*, 161, Huo, H., Wang, X., Yang, V., A general study of counterflow diffusion flames at subcritical and supercritical conditions: Oxygen/hydrogen mixtures, with Permission from Elsevier.

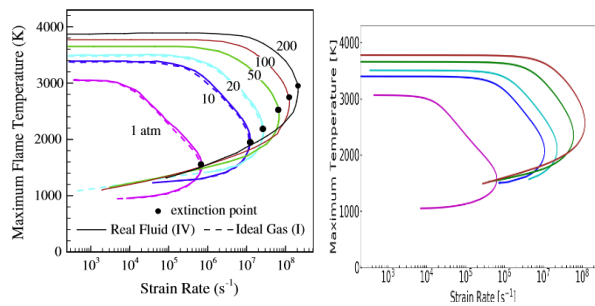


Figure 24. Comparison of strain rate vs. maximum flame temperature between Wang et al. [11] (left) and the in-house model (right). Wang et al. uses Li et al. [12] mechanism, whereas the in-house model uses Burke et al. [13] Reprinted from *Combustion and Flame*, 161, Huo, H., Wang, X., Yang, V., A general study of counterflow diffusion flames at subcritical and supercritical conditions: Oxygen/hydrogen mixtures, with Permission from Elsevier.

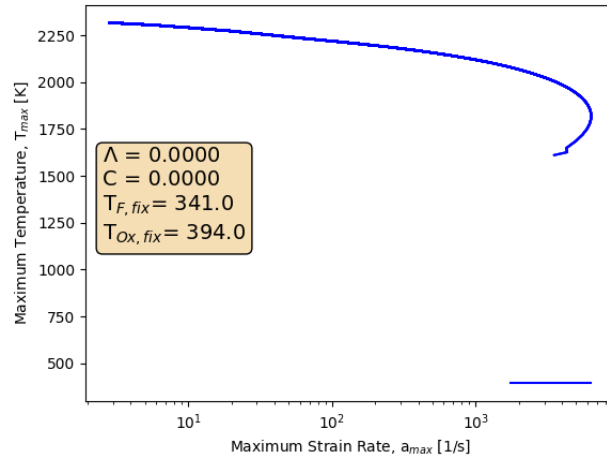


Figure 5. POSF10325-air diffusion flame s-curve.

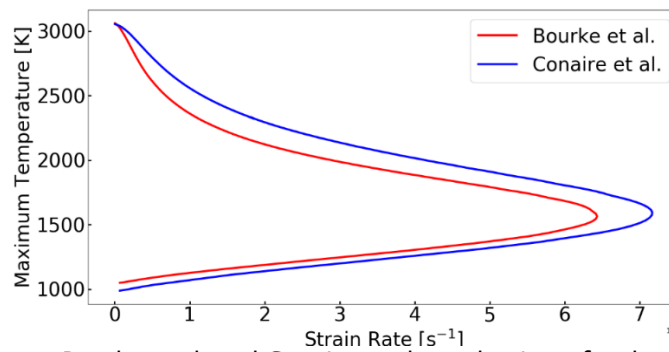


Figure 29. Comparison between Bourke et al. and Conaire et al. mechanisms for the H₂-O₂ flame at 1 atm and inlet temperatures of 300K.

I. Probability Density Functions

Here the Dirac-delta and Beta probability density functions (PDFs) are discussed here. These PDFs could be applied to either the lower-dimensional manifold variables. However, it has been proven that the Beta PDF is more suitable for mixture fraction (Z), whereas Dirac-delta or Beta PDF can be used for progress parameter (Λ).

1. Dirac Delta

The Dirac-delta probability density function is given by the equation below. Dirac-delta could be used for the progress parameter. Hence the x in the equation can be substituted by Λ .

$$\delta(x - x_0) = \begin{cases} 0, & x \neq x_0 \\ 1, & x = x_0 \end{cases} \quad (32)$$



2. Beta

The Beta probability density function is given by the equations below. The probability density function is appropriate for the mixture fraction (Z). Hence, the x in the equation can be substituted for the Z. This PDF could also be utilized to model the progress parameter and the x below would be substituted by Λ .

$$\beta(x; \bar{x}, \overline{x^2}) = \frac{\Gamma(a+b)}{\Gamma(a)\Gamma(b)} x^{a-1} (1-x)^{b-1} \quad (33)$$

$$a = \frac{\bar{x}(\bar{x} - \overline{x^2} - \overline{x^2})}{\overline{x^2}} \quad (34)$$

$$b = \frac{(1-\bar{x})(\bar{x} - \overline{x^2} - \overline{x^2})}{\overline{x^2}} \quad (35)$$

The demonstration of these convolutions are shown in Figure. The images correspond to a convoluted methane-air diffusion flame. Dirac-delta PDF was used for the progress variable. Note that the effect of turbulence-chemistry interaction represented by the variance of the mixture fraction (in this case) is to weaken the flame by lowering the peak temperature from ~2050 K to ~1750K. Similar the peak progress variable source term drops from ~500 to ~100 $\text{ks/m}^3\text{s}^{-1}$.

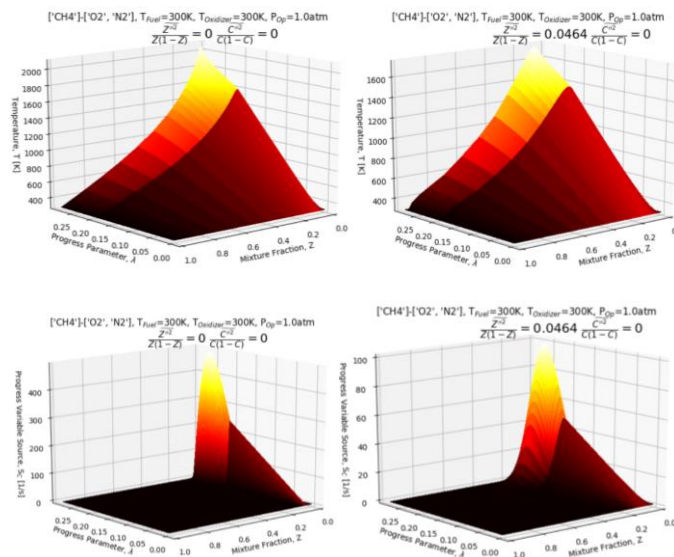


Figure 30. Sample images of a tabulated thermochemical transport tables for a CH₄-air diffusion flame. The top and bottom images illustrate temperature and progress variable source, respectively. The left images show the tabulated variables when both mixture fraction and progress variables are zero. The right images show the tabulated variables when the mixture fraction variance is non-zero.

J. Verification Tests

There are several verification and validation tests. A canonical laminar triple flame was computed using FPI or FPV models. The Sandia D piloted flame was also simulated using RANS/FPV and LES/FPV model. Finally, a single cup combustor rig was simulated using the LES/FPV model.

A. Simulations of a Canonical Triple Flame

Here is the verification test for the laminar formulation for the FPI model. Figure indicates that both calculations are very similar in terms of temperature and CO mass fraction contours. Subtle difference can be attributed to the fact that Wu et al. [9] used FlameMaster solver [10], which computes the flamelets in mixture fraction space directly.

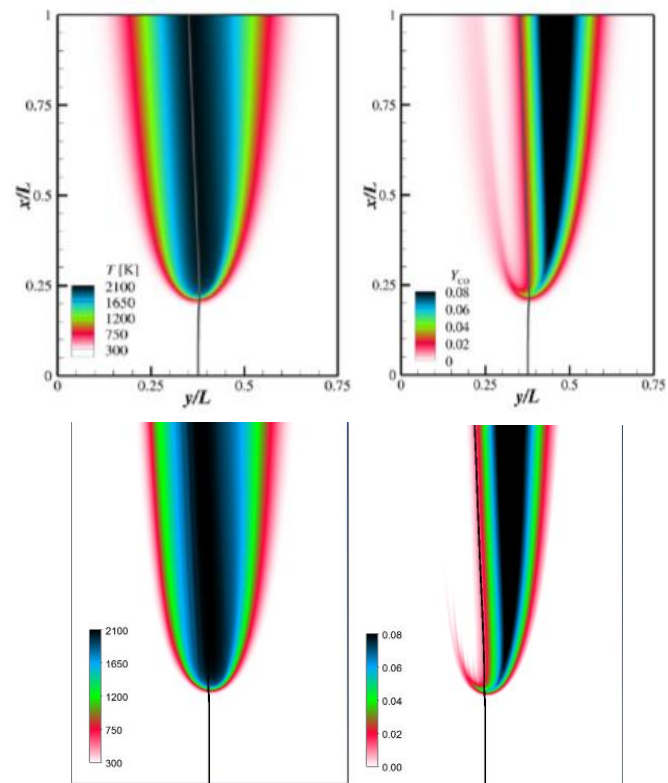


Figure 31. Comparison between (top) Wu et al. [15] and (bottom) CFR results of a laminar triple flame using FPI in terms of (left) temperature and (right) CO mass fractions.



B. Laminar Fpv Simulations For A Canonical Triple Flame

Here is the verification test for the laminar formulation for the FPV model. Figure illustrates the verification step for computing the laminar version of the FPV combustion model of the CFR software.

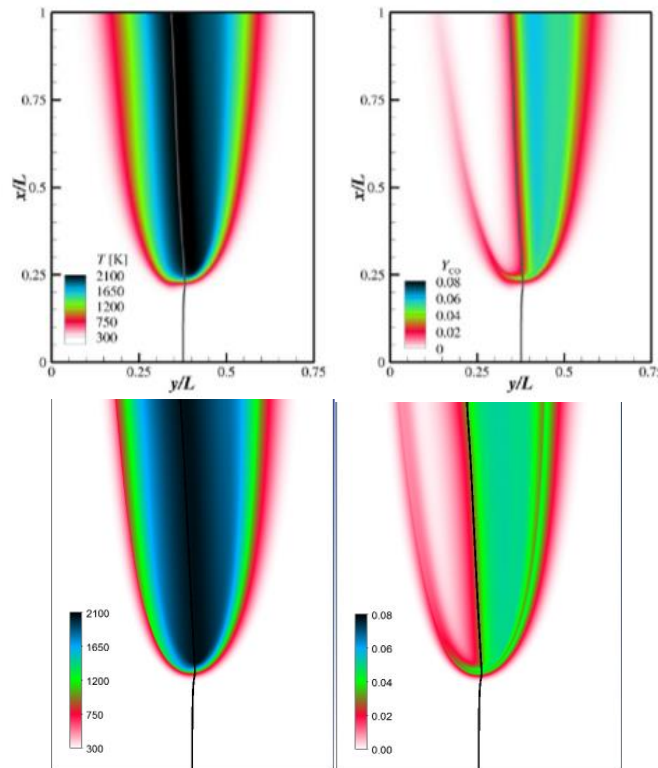


Figure 32. Comparison between (top) Wu et al. [15] and (bottom) CFR results of a laminar triple flame using FPV in terms of (left) temperature and (right) CO mass fractions.

C. Turbulent Simulations of Sandia D Flame

Here are the verification and validation tests for turbulent formulation of the FPV model. Figure 33 presents the experimental measurements against numerical predictions. Numerical simulations were performed only with Fluent [1,2] and with Fluent+CFR software. The $k-\epsilon$ and $k-\omega$ RANS version of FPV model were utilized. The Beta PDF is used for mixture fraction and Dirac-delta is used for progress variable. Generally, both the Fluent and Fluent+CFR results compared well with the experimental measurements in terms of temperature and species mass fractions. However, the Fluent+CFR outperforms the Fluent results, specifically, in terms of CO mass fraction. Both Fluent and Fluent+CFR results, nonetheless, underpredict the mixture fraction variance. In terms of RANS model, the $k-\omega$ better approximates the measurements.

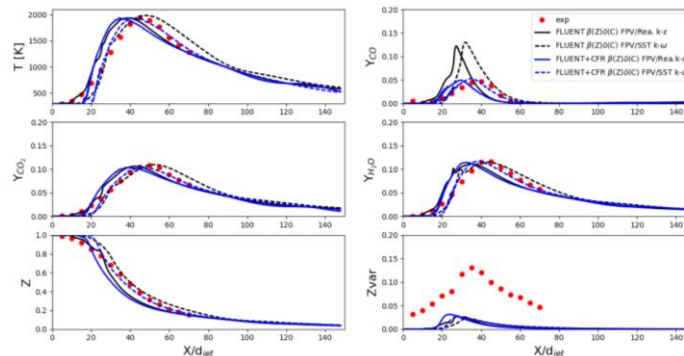


Figure 33. Centerline comparison between experiments and RANS simulations of the Sandia D turbulent flame.

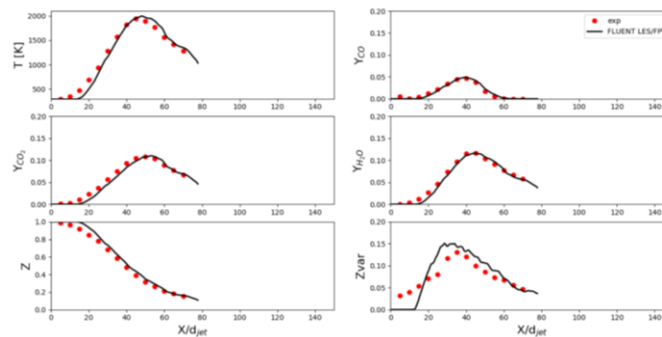


Figure 34. Centerline comparison between experiments and LES simulations of the Sandia D turbulent flame.

Conclusions

A common format routine (CFR) software for modeling combustion problems have been developed. This software is subdivided into a thermochemical transport property pretabulator software and a flamelet-based software. The former can be used to create flamelet prolongation of the ILDM (FPI) or flamelet/progress variable (FPV) tables for either laminar or turbulent flames. The pretabulator allows for turbulence-chemistry interaction through either Beta or Dirac-delta probability density function (PDF) of the independent variables. The flamelet-based software can read, search and interpolate the table to extract thermochemical and transport composition based on lower-dimensional manifold transport variables (i.e., mixture fraction, mixture fraction variance and progress parameter). The $k-\epsilon$ and $k-\omega$ RANS, SAS, DES and LES turbulence model were coupled with the flamelet-based combustion models. A multiphase spray model successfully couples with the gas phase by exchanging mass. The CFR software was positively compared against laminar and turbulent flames in canonical configurations as well as in more practical single-swirler combustor rig. The developed software is reliable for modeling and simulation of complex combustion phenomena.

References

Ansys Inc., Fluent User's Guide, v18.0.

Ansys Inc., Fluent Theory Guide, v18.0.

Goodwin, D.G., Moffat, H.K., Speth, R.L., Cantera: An object - oriented software toolkit for chemical kinetics, thermodynamics, and transport properties," <http://www.cantera.org>, 2017, Version 2.3.0. doi:10.5281/zenodo.170284

ANSYS 18.0, Chemkin-Pro Theory Manual, ANSYS, Inc.: San Diego, 2017.

Ihme, M., Pitsch, H., "Prediction of extinction and reignition in nonpremixed turbulent flames using flamelet/progress variable model: 2. Application in LES of Sandia flames D and E," *Combustion and Flame*, 155, (1-2), pp. 90-107, 2008.



- Fiala, T., Sattelmayer, T., "Nonpremixed Counterflow Flames: Scaling Rules for Batch Simulations," *Journal of Combustion*, 2014, 484372.
- H. B. Keller, in *Applications of bifurcation Theory*, P. Rabinowitz, Ed. (Academic Press, New York, 1977).
- Luigi Acampora and Francesco S. Marra, "Numerical Strategies for the Bifurcation Analysis of Perfectly Stirred Reactors with Detailed Combustion Mechanisms," *Computers and Chemical Engineering* 82 (2015) 273-282.
- Ruiqin Shan, Tianfeng Lu, Effects of Surrogate Jet-Fuel Composition on Ignition and Extinction in High Temperature Applications, 8th U. S. National Combustion Meeting Organized by the Western States Section of the Combustion Institute and hosted by the University of Utah May 19-22, 2013.
- Nishioka, M., Law, C., Takeno, T., "A flame controlling continuation method for generating S-curve responses with detailed chemistry," *Combust. Flame* 104 (3):328-342
- Huo, H., Wang, X., Yang, V., "A general study of counterflow diffusion flames at subcritical and supercritical conditions: Oxygen/hydrogen mixtures," *Combustion and Flames*, 161, 2014.
- J. Li, Z. Zhao, A. Kazakov, F.L. Dryer, "An updated comprehensive kinetic model of hydrogen combustion," *Int. J. Chem. Kinetics*, 36, 2004, 566-575.
- Burke, M.P., Chaos, M., Ju, Y., Dryer, F.L., Klippenstein, S.J., "Comprehensive H₂/O₂ Kinetic Model for High-Pressure Combustion," *Int. J. Chem. Kinet.* (2011).
- Connaire, M. O., Curran, H.J., Simmie, J. M., Pitz, W. J. and Westbrook, C.K., "A Comprehensive Modeling Study of Hydrogen Oxidation", *International Journal of Chemical Kinetics*, 36:603-622, 2004.
- Wu, H., See, Y.C., Wang, Q., and Ihme, M., "A Pareto-efficient combustion framework with submodel assignment for predicting complex flame configurations," 162(1), 2015, 4208-4230.
- Pitsch, H., FlameMaster v3.1, "A C++ computer program for 0D combustion and 1D laminar flame calculations," 1998.

Milestone(s)

Development of a stand-alone CFR.
OEMs have used the CFR internally.

Major Accomplishments

Developed and delivered to OEMs a stand-alone common format routine incorporating the latest theory from academic teams.

Publications

Nothing to report. A paper is in preparation.

Outreach Efforts

None.

Awards

Joshua Heyne - SOCHE Faculty Excellence Award, 2016.

Student Involvement

None.

Plans for Next Period

We plan to continue our current path with OEM participation continuing to increase with collaborations on simulating the Referee Rig with the developed CFR.

CFR APPENDIX

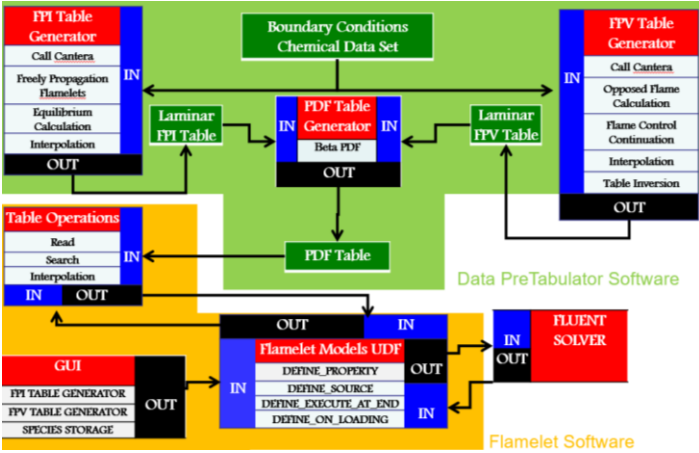


Figure A 1. Schematic of the Common Format Routine (CFR) software. All the components with the green background correspond to the thermochemical and transport data pretabulator. All the components with the amber background corresponds to the flamelet-based software.

Mixture Fraction

Element	Composition
O	<input type="checkbox"/>
H	<input checked="" type="checkbox"/>
C	<input checked="" type="checkbox"/>
N	<input type="checkbox"/>
Ar	<input type="checkbox"/>

Num variance

Figure A 2. Pretabulator software selection of user’s mixture fraction definition is indicated within the magenta-line box.

Progress Variable

Species Name	Composition
H2	<input checked="" type="checkbox"/>
H	<input type="checkbox"/>
O	<input type="checkbox"/>
O2	<input type="checkbox"/>
OH	<input type="checkbox"/>

Skip number Delta
 Beta
 SMLD

Num variance

Figure A 3. Pretabulator software selection of user’s progress variable definition is indicated within the magenta line box.

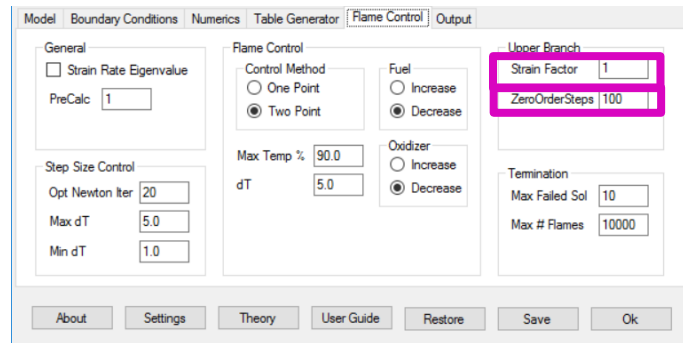


Figure A 4. Pretabulator software selection of zero order continuation steps and strain factor are indicated in the magenta boxes.

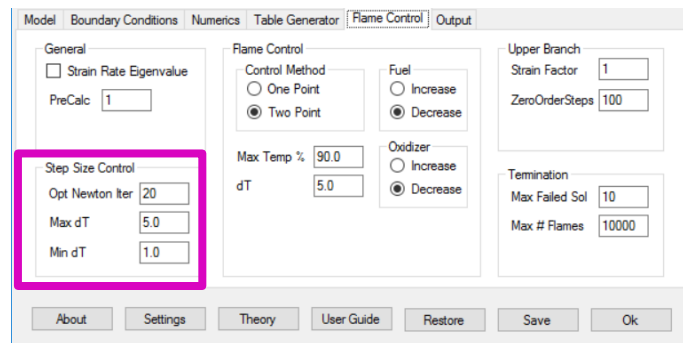


Figure A 5. Pretabulator software selection of step size control is indicated in the magenta box.

Task #5: Spray Modeling of Area 3 Pressure Atomized Spray Injector

Joshua Heyne
Vaidya Sankaran

Objective(s)

The objective of this task is to simulate the Area 3 High Sheer Rig pressure blast spray atomizer. Simulations of NJFCP experiments in the Area 3 High Sheer Rig will be done to explore the relative performance of simulations versus experiments and the relative spray and combustor character between the A-2, C-1, and C-5 fuels. These computational results will also illuminate the relative impact of a Pratt & Whitney swirler-injector geometry as compared to the other geometries in the program.

Research Approach

Large Eddy Simulations of the Area-3 Georgia Tech High Sheer Rig have been conducted. As an initial step to validate the grid resolutions, boundary conditions, numerical and physical model used in the simulation, non-reacting calculations are performed. Figure 35 shows the mean axial velocity contours, and Figure 38 a) is a series of line plots which are in very good agreement with experimental data.

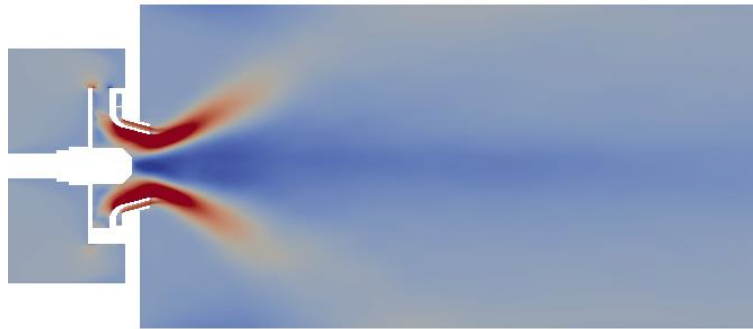


Figure 35: Mean axial velocity contours for Area 3 rig. Good prediction of the central & corner recirculation zones due to swirling flow-field Wall models are needed for resolving swirler walls which are not used here.

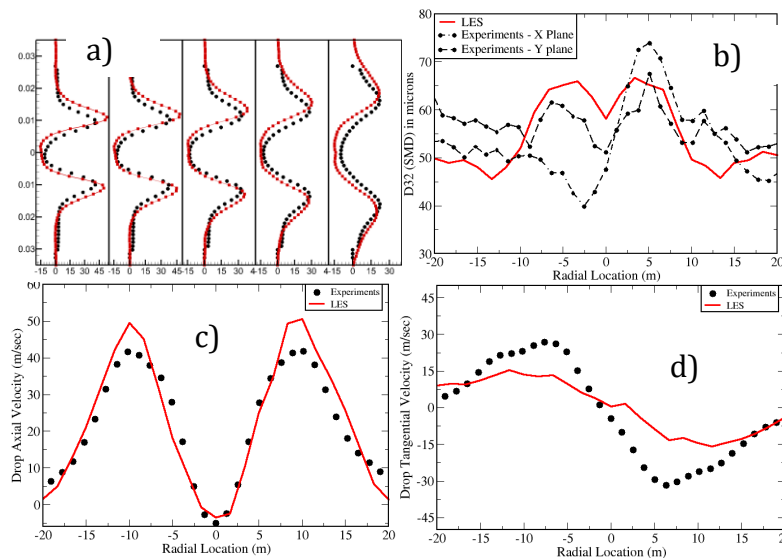


Figure 36: Line plot comparing a) mean axial velocity profiles, b) spray size, c) spray axial velocity, and d) spray tangential velocity for Georgia Tech data (solid circles) and UTRC simulations (red line). The simulations mimic the Georgia Tech data well by matching maximums, minimums, and overall maximums.

Since spray boundary conditions play a key role in reacting simulations, we also have performed another intermediate simulation where the measured spray data at a downstream location was projected back to the injector face and used as spray boundary conditions. Results from that simulations were then compared with measured data at downstream location to ascertain the validity of this approach. As shown in the line plots Figure 38, b) SMD, c) mean droplet axial velocity, and d) mean tangential velocities were predicted very well in this approach. As a final step, reacting simulations were performed with the A2 and C1 fuels using the previously validated models. The images of instantaneous and time-averaged temperature contours and mean reaction rate contours are shown in Figures 39 and 40 below.

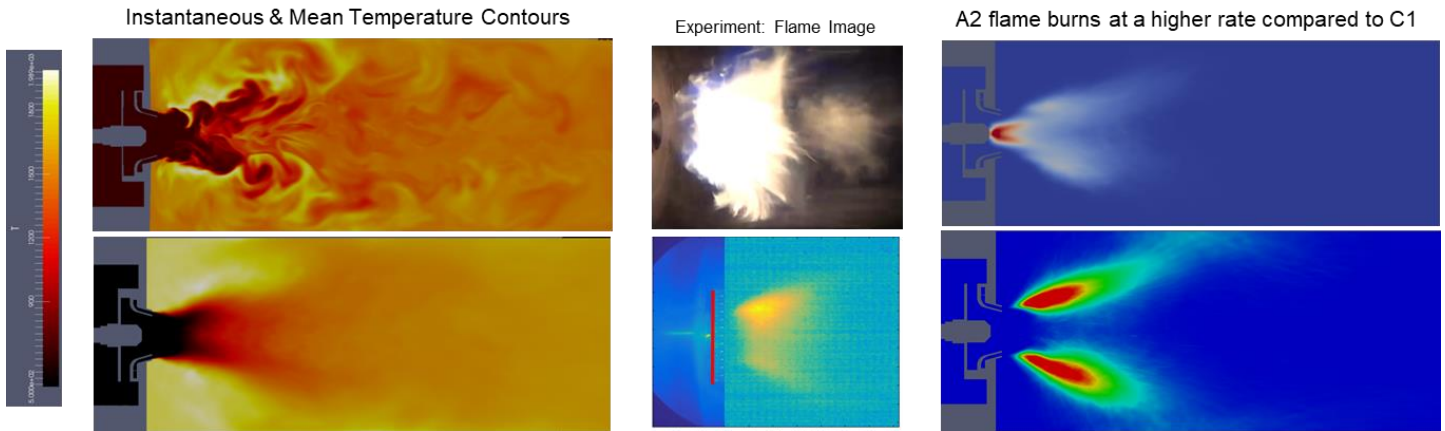


Figure 37: Comparisons of instantaneous (top) and mean (bottom) temperature (far left images) and heat release rates (far right images) for the nominal jet fuel (A-2). The middle images show a comparison of predicted vs. experimental results.

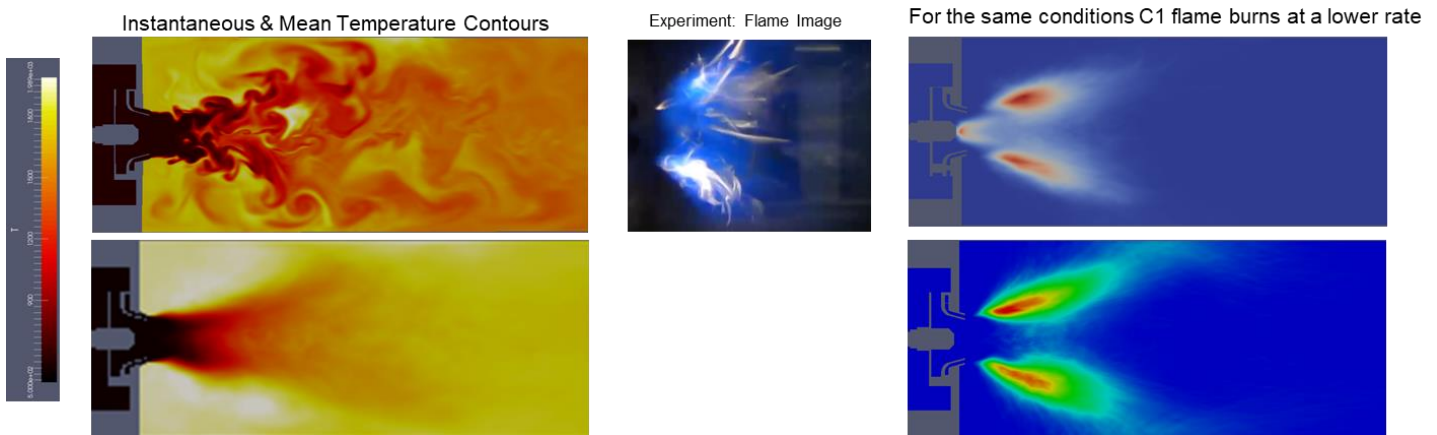


Figure 38: Comparisons of instantaneous (top) and mean (bottom) temperature (far left images) and heat release rates (far right images) for an alternative jet fuel (C-1).

While the temperature contours do not show significant differences between the two fuels, the reaction rate contours show that the C-1 flame is weaker than the A-2 flame, an initial marker of LBO. This is qualitatively consistent with the observed LBO behavior.

Milestone(s)

Execution of sub-contract.

Simulation of multiple fuels for the swirler and nozzle configuration at Georgia Tech.

Major Accomplishments

Comparisons of experiments and simulation results.

Publications

Nothing to report.

Outreach Efforts

Nothing to report.



Awards

Joshua Heyne - SOCHE Faculty Excellence Award, 2016.

Student Involvement

None.

Plans for Next Period

LBO simulations are being conducted to assess the impact of fuel on the LBO phenomena. UTRC to deliver final report on Area 3 spray simulations in Spring 2018.

Task #6: Procure Additional Geometries for Testing at Various NJFCP Facilities

Joshua Heyne
Scott Stouffer

Objective(s)

As seen earlier in this report, combustor geometry is an important sensitivity parameter in alt. jet fuel certification. For this reason, the NJFCP is interested in additional geometries for testing and constraining expectations from alt. fuels. Here we will procure these additional geometries for testing at various NJFCP facilities.

Research Approach

We have contacted a vendor capable of manufacturing the necessary hardware.

Milestone(s)

Nothing to report.

Major Accomplishments

Nothing to report.

Publications

Nothing to report.

Outreach Efforts

Nothing to report.

Awards

Joshua Heyne - SOCHE Faculty Excellence Award

Student Involvement

None.

Plans for Next Period

Order and acquire additional geometries from vendors.



Task #7: Ignition Testing of Conventional and Alternative Jet Fuels

Joshua Heyne
 Scott Stouffer
 Tyler Hendershott
 Jeffery Monfort

Objective(s)

The objective of this task is to measure the ignition probabilities of alternative and conventional jet fuels. The result of these tests are used to inform OEMs on the controlling physics in the Referee Rig at relevant conditions.

Research Approach

The Referee Rig is designed to mimic some of the most fuel sensitive engine combustor configurations while maintaining a relatively low cost size and operation. Previously, this rig has been used to test Lean Blowout (LBO) characteristics for various alternative and conventional jet fuels in the NJFCP and other programs. Here ignition probabilities are reported for the Referee Rig for a best, nominal, and worst case conventional fuel as well as one alternative fuel that was shown to have deleterious LBO behavior, see Figure and Figure .

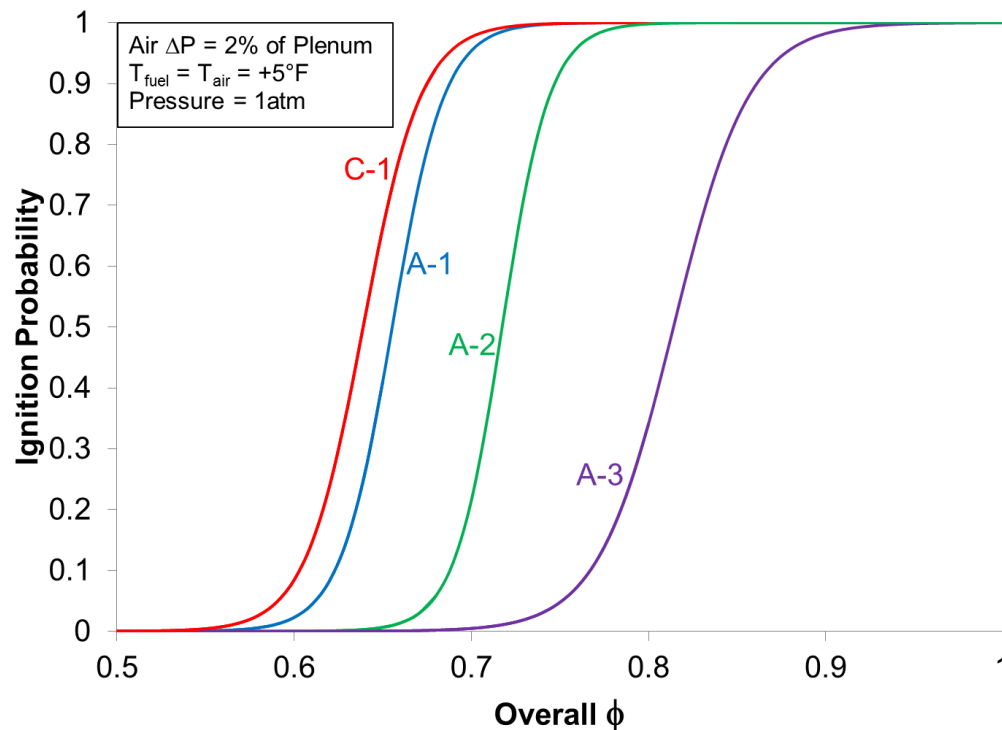


Figure 39: Ignition probabilities for the three conventional fuels as well as C-1, the alternative fuel with the worst LBO performance, at $\Delta P = 2\%$, $T_{fuel}/T_{air} = 5$ F, and $P=1$ atm. Significantly different ignition probabilities were observed for the conventional fuels. The alternative fuel C-1 is observed to have better ignition behavior than all the conventional fuels.

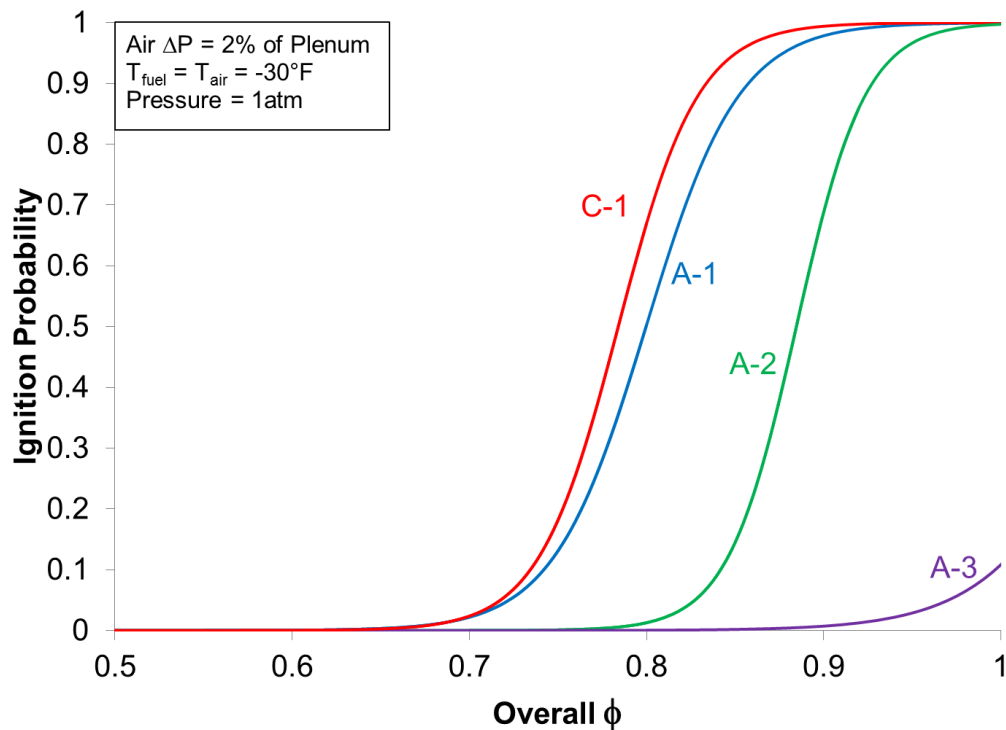


Figure 40: Ignition probabilities for the three conventional fuels as well as C-1, the alternative fuel with the worst LBO performance, at $\Delta P = 2\%$, $T_{fuel}/T_{air} = -30\text{ F}$, and $P=1\text{ atm}$. The overall ϕ required for an equivalent ignition probability for this temperature condition is significantly larger. Additionally, the fuel sensitivity is increased at the lower temperatures.

These data show that significant differences in ignition probabilities exist for conventional fuels. Where as in LBO, conventional fuels showed very similar LBO limits. Further, the fuel effects, i.e. the relative differences between fuels, is greater at lower temperatures. This implies a temperature dependent variable such as viscosity is driving the differences between fuels.

Milestone(s)

The generation of cumulative distribution functions for the various conventional and alternative jet fuels in the Referee Rig at cold conditions.

Major Accomplishments

Demonstrating significant fuel sensitivity in ignition probability for various fuels.

Publications

None.

Outreach Efforts

Presentation and poster at ASCENT Fall 2017.

Awards

None.

Student Involvement

None.



Plans for Next Period

We plan to pursue additional Referee Rig ignition studies via:

1. Further ignition experiments at fuel/air temperatures down to -30°F at atmospheric pressure,
2. Ignition experiments at pressures as low as 0.3 atm, and
3. Implementation of advanced optical diagnostics.